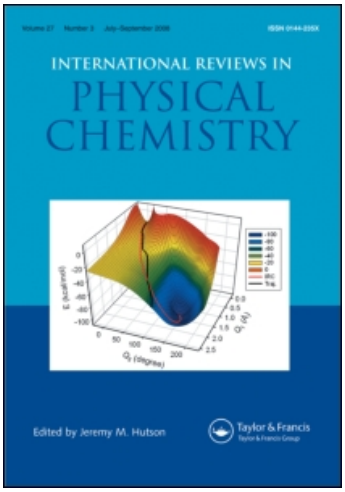

International Reviews in Physical Chemistry
Publication details, including instructions for authors and subscription information:
http://www.informaworld.com/smpp/title~content=t713724383

Potential energy surfaces and predicted infrared spectra for van der Waals complexes: dependence on one intramolecular vibrational coordinate

Daiqian Xie[a]; Hong Ran[a]; Yanzi Zhou[a]
[a] Institute of Theoretical and Computational Chemistry, Key Laboratory of Mesoscopic Chemistry, School of Chemistry and Chemical Engineering, Nanjing University, Nanjing 210093, China

To cite this Article Xie, Daiqian , Ran, Hong and Zhou, Yanzi(2007) 'Potential energy surfaces and predicted infrared spectra for van der Waals complexes: dependence on one intramolecular vibrational coordinate', International Reviews in Physical Chemistry, 26: 3, 487 — 520
To link to this Article: DOI: 10.1080/01442350701437926
URL: http://dx.doi.org/10.1080/01442350701437926

International Reviews in Physical Chemistry
Vol. 26, No. 3, July–September 2007, 487–520

Taylor & Francis
Taylor & Francis Group

Potential energy surfaces and predicted infrared spectra for van der Waals complexes: dependence on one intramolecular vibrational coordinate

DAIQIAN XIE*, HONG RAN and YANZI ZHOU

Institute of Theoretical and Computational Chemistry, Key Laboratory of Mesoscopic Chemistry, School of Chemistry and Chemical Engineering, Nanjing University, Nanjing 210093, China

(*Received 27 March 2007; in final form 7 May 2007*)

Involving the intramolecular vibrational coordinates in the potential energy surfaces and bound states calculations for van der Waals complexes is essential for fully predicting the infrared spectra of the complexes. In this review, we have summarized our recent researches on the potential energy surfaces and predicted infrared spectra of the van der Waals complexes containing a linear molecule and a rare-gas atom or H_2 by explicitly involving the dependence of one intramolecular vibrational coordinate related to the transitions in the infrared spectra. By incorporating the potential-optimized discrete variable representation grid points for that coordinate in both potential energy surfaces and bound states calculations for the Kr–H_2, He–N_2O, H_2–N_2O, and H_2–CO_2 complexes, the shift of the band origin, transition frequencies, and line intensities in the observed infrared spectra are reproduced well. Examples of other studies, Ar–HF and H_2–OCS, are also reviewed briefly.

Contents

*Corresponding author. Email: dqxie@nju.edu.cn

International Reviews in Physical Chemistry
ISSN 0144–235X print/ISSN 1366–591X online
http://www.tandf.co.uk/journals
DOI: 10.1080/01442350701437926

1. Introduction

van der Waals (vdW) complexes have attracted considerable theoretical and experimental attention because of the importance of vdW interactions in chemistry, physics, and molecular biology. The spectroscopy of these complexes provides very useful information for the intermolecular potential energy surface (IPES) and the dynamics of these weakly bound molecules. Due to the weak intermolecular forces in vdW complexes, the intermolecular vibrational modes have large amplitudes and low frequencies so that the global potential energy surface (PES) is required for the determination of the rovibrational bound states and for the prediction of the rovibrational spectra. On the other hand, the quality of the PES can also be justified by comparing the predicted spectra with the high-resolution spectra of the complexes.

Most theoretical studies have focused on the IPESs of the complexes containing a linear molecule monomer by taking the monomer as a rigid rotor [1, 2]. Since the vibrational energy of the monomer is at least two orders of magnitude larger than the energy of the intermolecular vibration, the inter- and intramolecular vibrations may be separated under some circumstances. This allows a Born–Oppenheimer-like separation between the inter- and intramolecular vibrational motions. The rigid monomer model is generally appropriate for the microwave spectra, which involve only the ground vibrational state of the linear molecule. However, it might not be sufficient for predicting the infrared spectra as the transition in at least one intramolecular vibrational mode is involved. In particular, the shift of the band origin in the observed infrared spectra cannot be correctly reproduced using the rigid monomer model [3].

An improved approach is to take into account the dependence of the intramolecular vibrational coordinate in the potential and dynamical calculations [4–13]. Because of their huge computational demands, theoretical studies involving the dependence of the intramolecular vibrations remain challenging. Since the

number of vdW complexes studied by *ab initio* and bound states calculations is very rapidly expanding, we will not try to summarize all the theoretical developments and applications in this review. Instead, we focus on our recent studies on the PESs and predicted infrared spectra for vdW complexes containing a linear molecule and a rare-gas (Rg) atom or H_2 by explicitly involving the dependence of one intramolecular vibrational coordinate which is related to the transition in the infrared spectra. The fundamental approach of our studies is to incorporate the potential-optimized discrete variable representation (PODVR) grid points in both PES and rovibrational bound states calculations without separating the inter- and intramolecular nuclear motions. The details of the approach used in our studies and its applications to the Kr–H_2, He–N_2O, H_2–N_2O, and H_2–CO_2 complexes are summarized in the following sections. Examples of other work, Ar–HF and H_2–OCS, are also reviewed briefly.

2. Rg–(linear molecule) vdW complexes

2.1. *General perspective*

For a weakly bound vdW complex involving a linear molecule and a Rg atom, the usual theoretical model is to treat the linear molecule as a rigid rotor. In this way, only two degrees of freedom (R, θ), where R is the distance between the Rg atom and the centre of mass of the linear molecule and θ is the enclosed angle between the vector $\boldsymbol{R}$ and the linear molecule, are required to be included in the construction of the IPES and in the calculations of the rovibrational bound states and spectra. The earlier methods of determining the rovibrational states of the atom–diatom vdW systems are the close-coupling approach in the space-fixed (SF) [4] or body-fixed (BF) [5] frame and the collocation method [14]. Most of the recent studies are based on the discrete variables representation (DVR) [15]. Choi and Light [16] proposed an efficient and accurate method using the DVR to treat the rovibrational states of Ar–HCl.

The supermolecular approach is usually used to produce the intermolecular potential energy, which is defined as the difference between the energy of the vdW complex and the sum of the monomer energies. It is believed that an accurate PES for a closed-shell vdW complex could generally be constructed using the single and double excitation coupled-cluster theory with a noniterative perturbation treatment of triple excitations [17] [CCSD(T)] with a large basis set, although valuable insights could be also obtained employing the fourth-order Møller–Plesset (MP4) perturbation theory in some cases. One common approach is to use the augmented correlation-consistent n-zeta (aug-cc-pVnZ) basis set of Woon and Dunning [18, 19] supplemented with an additional set of bond functions [20–24]. The bond functions are usually placed in the mid-point of the R vector to eliminate the need for higher angular momentum functions in the atom-centred basis set. The full counterpoise procedure [25] (FCP) is employed to correct the basis set superposition error (BSSE). Complementary to the supermolecular approach is the symmetry-adapted perturbation theory (SAPT) method [26–28], in which the interaction energy between two monomers is expanded perturbatively in powers of the intermolecular interaction operator. When truncated at the second order,

the interaction energy is decomposed into four physically interpretable components: electrostatics, induction, dispersion, and exchange. Current state of the art of the *ab initio* theory of vdW interactions has been reviewed in detail previously [3].

One of the early *ab inito* IPESs was constructed for He–HF [29] in 1981, which was found [30] not to correctly reproduce the near-infrared spectrum of the complex. Subsequently, Moszynski *et al.* [31] obtained a high-quality IPES of He–HF with the SAPT method, and the calculated near-infrared spectrum [32] is consistent with the observed one. Up to now, high-quality *ab initio* IPESs for a larger number of complexes are available. Some recent examples are Ar–HF [33], Ar–HCl [34, 35], He–CO_2 [36, 37], He–OCS [38], Ar–OCS [39], Ne–OCS [40–42], He–N_2O [43–45], Ne–N_2O [46, 47], Ar–SH [48], Ne–HCN [49], Ar–, Kr–, and Xe–C_2H_2 [50], He–HCCCN [51], Ne–HCCCN [52], and Ar–HCCCN [53, 54]. The explicit dependence of the IPES on the intramolecular coordinate is essential to the prediction of the infrared spectra, vibrational predissociation, or intramolecular vibrational redistribution. One of the earliest studies including intramolecular vibrational dependence was the work of Le Roy and van Kranendonk [4]. They obtained empirical three-dimensional anisotropic intermolecular potentials for the vdW complexes between Rg and H_2 by fitting to the near-infrared spectra of McKellar and Welsh [55] with a secular determinant method. Tennyson and Sutcliffe [5] derived an exact Hamitonian for atom–diatom systems by fully involving the vibration–rotation coupling and applied it to the Ne–H_2 and He–HF [56] complexes. Since then, there have been numerous studies in which the intramolecular vibrational dependence was included explicitly. The full-dimensional PESs of high accuracy are available for several Rg–diatom complexes, such as He–CO [7], Ar–CO [6], Ar–HF [57], He–O_2 [58], Ar–H_2 [59], and Kr–H_2 [60]. For diatom–diatom complexes, the PESs including all internal degrees of freedom of the system have been developed for $(HF)_2$ [61] and $(HCl)_2$ [62, 63]. In some cases, the off-diagonal inter- and intramolecular vibrational coupling is sufficiently small, so that one can use the potentials that are vibrationally averaged over the intramolecular coordinates to reduce the dimensionality to the intermolecular degrees of freedom. The idea of defining the vibrationally averaged potential was originated by Le Roy *et al.* [4, 64, 65]. It has been demonstrated for some vdW complexes, such as Ar–HF [9, 57, 66], Ar–HCl [67], He–CO [7], Ar–CO [6], He–OCS [38], that the surfaces constructed in this way could reproduce the observed spectroscopic properties very well.

2.2. *Hamiltonian and discretization*

The infrared spectra for a vdW complex usually involve a transition in an intramolecular vibrational coordinate Q. For a diatomic molecule, the vibrational coordinate Q is identical to the bond length r, while for a polyatomic linear molecule, Q can be taken as the normal mode which is responsible for the transition. Within Born–Oppenheimer approximation, the rovibrational Hamiltonian of the Rg–(linear molecule) complex in the Jacobi coordinates (R, θ, Q) at the BF frame can be

written [5, 68–70] (in atomic units) as,

$$\begin{aligned}\hat{H} = &-\frac{1}{2\mu_1}\frac{\partial^2}{\partial R^2} - \frac{1}{2\mu_2}\frac{\partial^2}{\partial Q^2} + \left(\frac{1}{2I_Q} + \frac{1}{2\mu_1 R^2}\right)\left(-\frac{1}{\sin\theta}\frac{\partial}{\partial\theta}\sin\theta\frac{\partial}{\partial\theta} + \frac{\hat{J}_z^2}{\sin^2\theta}\right) \\ &+ \frac{1}{2\mu_1 R^2}\left(\hat{J}^2 - 2\hat{J}_z^2\right) + \frac{\cot\theta}{2\mu_1 R^2}\left[\left(\hat{J}_x + i\hat{J}_y\right) + \left(\hat{J}_x - i\hat{J}_y\right)\right]\cdot\hat{J}_z \\ &+ \frac{1}{2\mu_1 R^2}\frac{\partial}{\partial\theta}\cdot\left[\left(\hat{J}_x + i\hat{J}_y\right) - \left(\hat{J}_x - i\hat{J}_y\right)\right] + V(R,\theta,Q),\end{aligned} \tag{1}$$

where μ_1 is the reduced mass of the Rg–(linear molecule) dimer, and μ_2 is the effective reduced mass for the vibrational mode Q of the linear molecule. I_Q is the rotational moment of inertia of the linear molecule, depending on Q. $\hat{J}_x$, $\hat{J}_y$ and $\hat{J}_z$ are the components of the total angular momentum vector $\hat{\boldsymbol{J}}$ in the BF frame, in which the z axis lies along the vector $\boldsymbol{R}$ and the complex is in the xz plane. The above Hamiltonian contains full inter- and intra-molecular vibration–rotation coupling. The three-dimensional PES can be divided as,

$$V(R,\theta,Q) = V_1(Q) + \Delta V(R,\,\theta,\,Q), \tag{2}$$

where $V_1(Q)$ is the potential energy curve of the isolated linear molecule and $\Delta V(R,\theta,Q)$ is the IPES between the linear molecule and the Rg atom. The total rovibrational wavefunction for a rovibrational state n can be expanded as

$$\Psi_n^{JMp}(R,\,\theta,Q,\alpha,\beta,\gamma) = \sum_{j,K,v_1,v_2} c_{j,K,v_1,v_2}^{nJp}\psi_{v_1}(R)\psi_{v_2}(Q)P_j^K(\cos\theta)C_{MK}^{Jp}(\alpha,\,\beta,\gamma), \tag{3}$$

where K and M are the projection of the total angular momentum J onto the BF and SF z axis, respectively. The parity adapted rotational bases $C_{MK}^{Jp}(\alpha,\,\beta,\,\gamma)$are defined in terms of the normalized Wigner rotational functions D_{MK}^J in the three Euler angles (α,β,γ) denoting the orientation of the BF frame with respect to the SF frame,

$$C_{MK}^{Jp}(\alpha,\,\beta,\,\gamma) = [2(1+\delta_{K0})]^{-1/2}[D_{MK}^{J*} + (-1)^{J+K+p}D_{M-K}^{J*}]. \quad p = 0,\,1. \tag{4}$$

The total parity is given by $(-1)^{J+p}$. $P_j^K(\cos\theta)$ are the normalized associated Legendre functions. Because of the large amplitude of the intermolecular vibrational motions and usually multiple minima in the PES with only low barriers between them, the basis set $\psi_{v_1}(R)$ for the coordinate R should be taken as a very flexible basis, such as Morse oscillator functions [5], distributed Gaussian basis [15], tridiagonal Morse basis [71], or sine basis [72]. $\psi_{v_2}(Q)$ are the vibrational wavefunctions for the mode Q of the linear molecule, which are obtained by solving the following one-dimensional Schrödinger equation

$$\left[-\frac{1}{2\mu_2}\frac{d^2}{dQ^2} + V_1(Q)\right]\psi_{v_2}(Q) = E_{v_2}\psi_{v_2}(Q). \tag{5}$$

The potential $V_1(Q)$ can be adjusted to get the calculated transition frequency for the mode Q in accord with the observed value. The finite basis representation (FBR) in equation (3) can be conveniently transformed to the DVR in the Jacobi coordinate (R, θ, Q), as described in [71–73]. Any local functions in the Jacobi coordinates are assumed to be diagonal in the DVR. The matrix elements of the Hamiltonian in the DVR are given by

$$\begin{aligned}
&\langle \alpha' \beta' q' K' | \hat{H} | \alpha \beta q K \rangle \\
&= \langle \alpha' | -\frac{1}{2\mu_1}\frac{\partial^2}{\partial R^2} | \alpha \rangle \cdot \delta_{\beta'\beta} \cdot \delta_{K'K} \cdot \delta_{q'q} + \langle q' | -\frac{1}{2\mu_2}\frac{\partial^2}{\partial Q^2} | q \rangle \cdot \delta_{\alpha'\alpha} \cdot \delta_{\beta'\beta} \cdot \delta_{K'K} \\
&\quad + \left(\frac{1}{2\mu_1 R_\alpha^2} + \frac{1}{I_{Q_q}} \right) \langle \beta' | \hat{j}^2 | \beta \rangle \cdot \delta_{\alpha'\alpha} \cdot \delta_{K'K} \cdot \delta_{q'q} + \frac{1}{2\mu_1 R_\alpha^2} \left\{ \left[J(J+1) - 2K^2 \right] \cdot \delta_{\beta'\beta} \cdot \delta_{K'K} \right. \\
&\quad - (1+\delta_{K0})^{1/2} \Lambda_{JK}^{+} \cdot \langle \beta' | \hat{\boldsymbol{j}}_{+} | \beta \rangle \cdot \delta_{K'K+1} - (1+\delta_{K'0})^{1/2} \Lambda_{JK}^{-} \cdot \langle \beta' | \hat{\boldsymbol{j}}_{-} | \beta \rangle \cdot \delta_{K'K-1} \\
&\quad + V(R_a, \theta_\beta^{(K)}, Q_q) \cdot \delta_{\alpha'\alpha} \cdot \delta_{\beta'\beta} \cdot \delta_{K'K} \cdot \delta_{q'q} \qquad (6)
\end{aligned}$$

where $\Lambda_{JK}^{\pm} = \sqrt{J(J+1) - K(K \pm 1)}$. The rovibrational energy levels and wavefunctions can be obtained by diagonalizing the above Hamiltonian matrix. One should note that the SF basis set could be used as well.

2.3. *Diagonalization of the Hamiltonian matrix*

Due to unfavourable scaling laws in both arithmetic operations and memory, the traditional methods for diagonalizing the symmetric matrix, such as Householder method [74], which generates the complete set of eigenvalues and eigenvectors, become inadequate when the number of basis functions is large. The Lanczos method [75, 76], which is a recursive method based on the Krylov subspaces [77], could be employed to efficiently diagonalize the Hamiltonian matrix in the DVR to produce the energy levels and wavefunctions of the rovibrational states [78–84]. The basic idea of the Lanczos method is to recursively generate a small number of vectors that span the eigenspace of interest. Because of the recursive nature, this method has favourable scaling laws. In this method [75], the Lanczos vector is updated by the following three-term recursion formula

$$\psi_{k+1} = \frac{[(\mathbf{H} - \alpha_k)\psi_k - \beta_{k-1}\psi_{k-1}]}{\beta_k} \quad k = 1, 2, \ldots \qquad (7)$$

with

$$\alpha_k = \psi_k^T (\mathbf{H}\psi_k - \beta_{k-1}\psi_{k-1}), \qquad (8)$$

$$\beta_k = \| (\mathbf{H} - \alpha_k)\psi_k - \beta_{k-1}\psi_{k-1} \|, \quad \beta_0 = 0 \qquad (9)$$

which forms the tridiagonal Lanczos matrix,

$$\mathbf{T}^{(K)} = \begin{pmatrix} \alpha_1 & \beta_1 & & 0 \\ \beta_1 & \alpha_2 & \beta_2 & \\ & \beta_2 & \ddots & \beta_{K-1} \\ 0 & & \beta_{K-1} & \alpha_K \end{pmatrix}. \tag{10}$$

The eigenvalues are generated by the diagonalization of the Lanczos matrix, and the ones near the spectral extreme converge relatively quickly. Since only low-lying rovibrational states for the vdW complexes are required to predict the infrared spectra when the vibrationally averaged PESs are used, the Lanczos method is particularly suitable in this case. In a fully coupled approach, due to high energy of the monomer vibrational excitation, a very large number of propagation steps are needed to generate the converged energy levels in the region of the excited vibrational state of the monomer. The Lanczos method requires only two vectors to be stored in the memory, since only the action of the Hamiltonian needs to be evaluated. The eigenfunctions can be obtained using additional Lanczos recursion with the eigenvectors determined in the first recursion. An implementation of the Lanczos method, used in our laboratory, has been reviewed previously [85].

2.4. *Fitting of the potential energy surface*

In order to interpret the observed infrared spectra of vdW complexes, only the first two vibrational states of the monomer molecule are of interest. On the other hand, the intramolecular vibration of the molecule has a much higher frequency than the intermolecular vibrations. Thus, only a few PODVR grid points for the coordinate Q are sufficient to represent the intramolecular vibration and lead to the converged rovibrational energy levels. Accordingly, the IPES $\Delta V(R, \theta, Q)$ could be constructed at these PODVR grid points, and the potential for other values of Q can be obtained by a polynomial interpolation when necessary. One advantage of constructing the PES in this way is that the potential at the coordinate Q is directly incorporated into the Hamiltonian in the DVR, thus the possible interpolation errors for Q could be avoided. The calculated *ab initio* potential energies can be represented with a cubic spline interpolation if the points are dense enough. Otherwise, one can fit them to an analytic form. A widely used form is as follows [51, 54, 86–88],

$$V(R, \theta, Q_i) = V_{sh}(R, \theta, Q_i) + V_{as}(R, \theta, Q_i), \tag{11}$$

where Q_i are the PODVR grid points for the coordinate Q. $V_{sh}(R, \theta, Q_i)$ denotes the short-range part of the potential and is assumed to be

$$V_{sh}(R, \theta, Q_i) = G(R, \theta, Q_i) e^{D(\theta, Q_i) - B(\theta, Q_i)R} \tag{12}$$

where $G(R, \theta, Q_i)$, $D(\theta, Q_i)$ and $B(\theta, Q_i)$ are expanded in terms of Legendre polynomials $P_l(\cos\theta)$,

$$G(R,\theta,Q_i) = R^{-1}\sum_{i=0}^{4} R^i \sum_{l=0}^{6} g_i^l(Q_i)\frac{(-1)^l P_l(\cos\theta)}{\sqrt{2l+1}}, \tag{13}$$

$$D(\theta,Q_i) = \sum_{l=0}^{4} d^l(Q_i)\frac{(-1)^l P_l(\cos\theta)}{\sqrt{2l+1}}, \tag{14}$$

$$B(\theta,Q_i) = \sum_{l=0}^{4} b^l(Q_i)\frac{(-1)^l P_l(\cos\theta)}{\sqrt{2l+1}}. \tag{15}$$

The long-range part $V_{as}(R,\theta,Q_i)$ is expressed as,

$$V_{as}(R,\theta,Q_i) = -\sum_{l,n} f_n[B(\theta,Q_i)R]\frac{C_n^l(Q_i)}{R^n}\frac{(-1)^l P_l(\cos\theta)}{\sqrt{2l+1}}, \tag{16}$$

where $f_n[x] = 1 - e^{-x}\sum_{k=0}^{n} x^k/k!$ is the Tang–Toennies damping function [89] to reduce the long-range part at short R.

2.5. *Calculation of the transition intensity*

The dipole moments of the complex in the BF frame can also be obtained from the electronic structure calculations. Since the complex in the BF frame is embedded in the xz plane, the component of the dipole moment along the y axis (μ_y) is equal to zero. The non-zero components of the dipole moment are denoted as μ_x and μ_z along the BF x and z axes, respectively. The intensity of a transition from an initial rovibrational state $|Jpn\rangle$ to a final state $\left|J'p'n'\right\rangle$ at a temperature T can be evaluated as [1, 90, 91],

$$I_{Jpn\to J'p'n'} \propto (E_{J'p'n'} - E_{Jpn})[e^{-E_{Jpn}/kT} - e^{-E_{J'p'n'}/kT}]\sum_{M}\sum_{M'}\sum_{A=X',Y',Z'}\left|\left\langle\Psi_n^{JMp}\middle|\mu_A\middle|\Psi_{n'}^{J'M'p'}\right\rangle\right|^2, \tag{17}$$

where n is the collective quantum number for the rovibrational state with the energy of E_{Jpn}, k is the Boltzmann constant, μ_A is the component of the molecular dipole moment operator along A axis ($A = X', Y', Z'$) of the SF frame, and M and M' are the rotational quantum numbers quantizing the Z' component of the total angular momentum of the initial and final states in the SF frame.

The components of the dipole moment, usually computed in the BF frame (x, y, z), can be rewritten as

$$\mu_{+1} = -\frac{1}{\sqrt{2}}(\mu_x + i\mu_y), \quad \mu_{-1} = \frac{1}{\sqrt{2}}(\mu_x - i\mu_y), \quad \mu_0 = \mu_z. \tag{18}$$

If one defines analogous quantities in the SF frame, μ'_g(the dipole moment in the SF frame) can be calculated from the following transformation

$$\mu'_g = \sum_{h=-1}^{1} \mu_h D^1_{gh}(\alpha, \beta, \gamma), \tag{19}$$

where D^1_{gh} are the Wigner rotational functions. The rovibrational wavefunction in equation (3) can be rewritten as

$$\Psi_n^{JMp}(R, \theta, Q, \alpha, \beta, \gamma) = \sum_K \Psi_K^{Jnp}(R, \theta, Q) C_{MK}^{Jp}(\alpha, \beta, \gamma) \tag{20}$$

The transition intensity can be then evaluated as

$$I_{Jpn \to J'p'n'} \propto (2J+1)(2J'+1)(E_{J'p'n'} - E_{Jpn})[e^{-E_{Jpn}/kT} - e^{-E_{J'p'n'}/kT}]$$
$$\left| \sum_K \sum_{K'} [(1+\delta_{K0})(1+\delta_{K'0})]^{-\frac{1}{2}} \sum_h \left\{ (-1)^K \begin{pmatrix} J & J' & 1 \\ -K & K' & h \end{pmatrix} + (-1)^{J+p} \begin{pmatrix} J & J' & 1 \\ K & K' & h \end{pmatrix} \right.\right.$$
$$\left.\left. + (-1)^{K+J'+p'+K'} \begin{pmatrix} J & J' & 1 \\ -K & -K' & h \end{pmatrix} + (-1)^{J+p+J'+p'+K'} \begin{pmatrix} J & J' & 1 \\ K & -K' & h \end{pmatrix} \right\} \int \Psi_K^{Jnp} \mu_h \Psi_{K'}^{J'n'p'} d\tau \right|^2 \tag{21}$$

where the symbols in large brackets are the Winger 3-j symbols.

2.6. *H_2–Kr*

Over the last 40 years, the H_2–Rg complexes have been prototype complexes for studying the intermolecular interactions and high-resolution spectroscopy [4, 10, 55, 59, 92–96]. Among the H_2–Rg complexes, much effort has been focused on the H_2–Ar complex, which is one of the most thoroughly studied atom–diatom complexes [1]. Williams *et al*. [97] have provided the first complete *ab initio* PES for H_2–Ar with the SAPT approach, which was subsequently used to calculate the rovibrational spectra of H_2–Ar and D_2–Ar [8]. The heavier species such as H_2–Kr and H_2–Xe are also interesting. In 1971, McKellar *et al*. [55] studied the high-resolution spectra of the H_2–Ar, H_2–Kr and H_2–Xe complexes and observed the spectra due to transitions

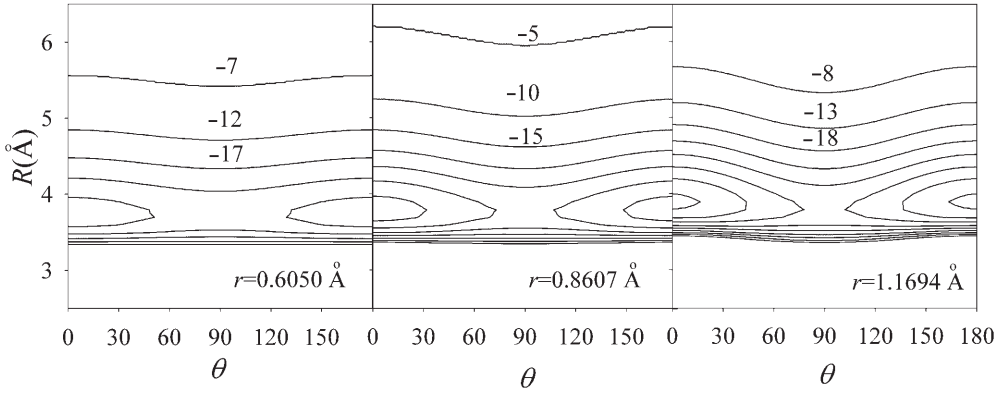

Figure 1. Contour plots of the intermolecular potential energy of H_2–Kr at fixed H_2 bond length ($r = 0.6050$, 0.8607, and 1.1694 Å). Contours are labelled in cm^{-1}.

in the D_2–Rg complexes. Very recently, McKellar [96] observed the high-resolution infrared spectra of H_2–Kr and D_2–Kr and assigned 219 measured line positions from the spectra. Wei *et al.* [98] have determined a reliable empirical three-dimensional PES for H_2–Kr by directly fitting to the observed infrared spectra using the exchange-Coulomb model for the intermolecular interaction energy. In addition, the experimental second virial and diffusion coefficients [99] were also used to confirm the high quality of the potential.

We [60] have constructed a three-dimensional *ab initio* PES of the H_2–Kr complex. The larger number of electrons makes H_2–Kr a more challenging task than the other lighter H_2–Rg complexes for *ab initio* calculations. The intermolecular potential energies were calculated using the CCSD(T) method with a large basis set including bond functions. Contour plots of three two-dimensional CCSD(T) IPESs for the H_2–Kr complex are displayed in figure 1. It is clear that the IPESs feature a collinear global minimum and an energy barrier at the T-shaped geometry. The intermolecular interaction between H_2 and Kr is strengthened for larger r. The global minimum for the three-dimensional PES has a collinear structure at $R = 3.7605$ Å and $r = 0.7422$ Å with a well depth of 61.76 cm^{-1}. The saddle point along the angular coordinate was located at $R = 3.7475$ Å, $r = 0.7421$ Å, and $\theta = 90^\circ$ with a barrier height of 12.12 cm^{-1}. Similar to the empirical three-dimensional PES [98], the *ab initio* PES for H_2–Kr has a very small angular anisotropy and a weak radial–angular coupling.

The rovibrational energy levels and wavefunctions up to $J = 6$ for the H_2–Kr complex were determined based on the *ab initio* PES. The potential supports only two intermolecular vibrational bound states. The calculated transition frequencies in the region of the H_2 fundamental vibrational band were calculated and compared with the experimental values [96]. Table 1 gives the calculated transition frequencies in the $Q_1(0)$ band of H_2–Kr together with the observed values. The experimental and calculated band origins were taken as the reference. It is shown that the discrepancies of the calculated transition frequencies are within 3% of the observed values. The calculated shift of the band origin relative to the vibrational frequency of isolated H_2 molecule was found to be -1.50 cm^{-1}, which is in very good agreement with the experimental value of -1.706 cm^{-1}.

Table 1. Calculated [60] and observed [96] transition frequencies in the $Q_1(0)$ band of H_2–Kr (in cm^{-1}). The transition frequencies are given with respect to the band origin. l is the end-over-end rotational quantum number.

$l' = J'$	$l = J$	Obs	Cal.	(Obs–Cal.)/Obs
5	6	−5.927	−5.773	2.6%
4	5	−5.041	−4.923	2.3%
3	4	−4.089	−4.000	2.2%
2	3	−3.098	−3.032	2.1%
1	2	−2.078	−2.035	2.1%
0	1	−1.039	−1.021	1.7%
1	0	1.035	1.019	1.5%
2	1	2.070	2.029	2.0%
3	2	3.084	3.020	2.1%
4	3	4.072	3.985	2.1%
5	4	5.025	4.911	2.3%
6	5	5.931	5.783	2.5%

2.7. *Ar–HF*

The Ar–HF complex has been an important prototype system in the study of weak intermolecular forces. Klemperer *et al.* [100, 101] observed the first radio-frequency and microwave spectra of Ar–HF in 1974 and Ar–DF in 1981 in the ground vibrational state using molecular beam electric resonance spectroscopy, and determined the structure of the complex. The microwave spectra of Ar–HF and Ar–DF were also measured using pulsed Fourier transform microwave spectroscopy in a molecular beam [102] and from a slit supersonic expansion with improved accuracy [103]. Rotational resolved infrared spectra of Ar–HF were respectively obtained by Lovejoy *et al.* [104–107] using difference frequency laser spectroscopy in a one-dimensional supersonic expansion, by Fraser and Pine [108] using the same technique in a gas cell, by Huang *et al.* [109] using optothermal molecular-beam spectroscopy, by Farrell *et al.* [110] using Nd:YAG/dye laser difference frequency generation, and by Chang *et al.* [111, 112] and Chuang *et al.* [113–115] using intracavity laser-induced fluorescence in a slit supersonic jet. In addition, Dvorak *et al.* [116] measured several bands in the far-infrared spectrum of Ar–HF ($v = 0$) using far-infrared laser spectroscopy in a slit jet. These spectroscopic investigations have provided a larger number of energy levels of the vdW stretching and bending modes and the intramolecular vibration of the HF monomer ($v = 0$–4).

The large body of spectroscopic data for Ar–HF made it possible to determine reliable empirical PES. Hutson and Howard [117] obtained the first two-dimensional IPES for Ar interacting with HF($v = 0$) by fitting to the microwave spectra of Ar–HF and Ar–DF. Nesbitt *et al.* [118] used the infrared spectra to obtain another IPES for Ar interacting with HF($v = 1$) by a novel direct inversion procedure. Hutson [9] constructed an accurate IPES including the vibrational dependence for Ar–HF by fitting to observed data from high-resolution microwave, far-infrared, and infrared spectroscopy. His three-dimensional PES H6(4, 3, 2) reproduces all the available spectroscopic data. Since then, this PES has been successfully employed to study the state-to-state rotationally inelastic scattering of Ar+HF [119, 120] and the properties of Ar_n–HF clusters [12, 121–131].

An early *ab inito* IPES of Ar–HF was obtained by Kolos *et al.* [132] using the self-consistent field (SCF) method. Chang *et al.* [112] constructed a three-dimensional PES of Ar–HF by the supermolecular approach using a large standard basis set augmented with bond functions with the MP4 method. The PES reproduces the anisotropy of the H6(4, 3, 2) potential and its vibrational dependence, and gives a well depth of 92–95% of that of the H6(4, 3, 2). Subsequently, Tao and Klemperer [22] investigated the IPES of Ar–HF with a fixed HF bond length at its vibrationally averaged value and further performed the calculations including the dependence of the HF bond length to generate vibrationally averaged IPES for $v = 0$–3. Lotrich *et al.* [33] determined a two-dimensional IPES of Ar–HF using the SAPT method with the H–F distance fixed at its equilibrium value. The *ab initio* SAPT potential agrees well with the empirical H6(4,3,2) potential of Hutson [9], including a reasonably similar behaviour of the anisotropy. The rovibrational energy levels calculated upon the SAPT potential are within $1\,cm^{-1}$ of the values predicted from the H6(4, 3, 2) potential for stretch-type states, while the levels of the states corresponding to bending vibrations agree to a few cm^{-1}. Later, the SAPT potential was used by Jeziorska *et al.* [57] to generate several two-dimensional potentials: the vibrationally averaged potential and the potentials obtained by fixing r at its equilibrium value r_e and at the vibrationally averaged distances. For these two-dimensional potentials, the rovibrational spectra were evaluated and compared with the spectra obtained upon the three-dimensional SAPT potential. It was found that the potential obtained by setting $r = \langle r \rangle$ performs much better than that corresponding to $r = r_e$, while the vibrationally averaged potentials are the most appropriate ones. The calculated shifts of the band origins (red-shifts) for vibrational excited $v = 1$ and $v = 2$ states upon the vibrationally averaged potentials were found to be 10.081 and $23.303\,cm^{-1}$, which are very close to the calculated values of 10.155 and $23.272\,cm^{-1}$ upon the full three-dimensional potential and the observed values of 9.655 [106, 108] and $20.913\,cm^{-1}$ [110].

Recently, Jankowski [66] proposed a method of generating the full-dimensional PES for vdW complexes, based on the local expansion of the exact interaction energy surface in the Taylor series with respect to intramolecular coordinates. This leads to significant savings in computations of the full-dimensional PES. He also suggested a method for the direct calculation of the vibrationally averaged IPES without explicit knowledge of the full-dimensional surface. He further used this approach to obtain the full-dimensional and vibrationally averaged PESs of Ar–HF with the supermolecular approach using the CCSD(T) method. It was turned out again that the vibrationally averaged PES is a very good approximation to the full-dimensional PES.

2.8. *He–N_2O*

N_2O is a precursor for the production of nitrogen oxides NO_x, which plays an important role in stratospheric ozone chemistry [133, 134]. It is also a key component in the atmosphere, which causes greenhouse effect [134]. The intermolecular interactions in vdW complexes containing He are very weak so that they usually exhibit complicated energy level patterns and spectra. Nauta and Miller [135] have reported the observed infrared spectra of N_2O in superfluid helium droplets which indicate strong droplet size dependence for the shift of the vibrational band origin. Xu *et al.* [136] have presented

high-resolution microwave and infrared spectra of He_n–N_2O clusters, raising interesting questions regarding to the effect of the bosonic helium environment on the behaviour of rotational constants and vibrational band origins. Tang and McKellar [137] have observed the infrared spectra of He–N_2O in the v_3 vibrational band of N_2O using a tunable diode laser to probe a pulsed supersonic jet expansion. They found that the ^{4}He–N_2O complex is close to an oblate symmetric rotor limiting case while ^{3}He–N_2O is an asymmetric rotor. Moreover, their infrared spectra showed that *a*-type ($\Delta K_a = 0$, K_a is the projections of J onto the *a* axis in the coordinates of principal axes of inertia) transitions are dominant for ^{3}He–N_2O, while both *a*-type and *b*-type ($\Delta K_a = \pm 1$) transitions are prominent for ^{4}He–N_2O.

Three two-dimensional *ab initio* IPESs and predicted spectra have recently been reported [43–45] by assuming the N_2O molecule as a rigid rotor. Chang *et al.* [43] have calculated a two-dimensional IPES of He–N_2O at the SAPT level and then computed the rovibrational energy levels of ^{4}He–N_2O upon the surface. By comparing with the *ab initio* IPES of He–CO_2 [36, 37, 138], they reasoned that the observed larger reduction of the N_2O rotational constants with respect to that of CO_2 in superfluid helium nanodroplets [135] might be related to the greater potential depth in the He–N_2O complex, resulting to a greater probability to attach the helium atoms. This IPES was further used to study the rovibtaional spectra of the He_2–N_2O [139] and He_n–N_2O [140] clusters. We [44] have studied the IPES at the CCSD(T) level of theory. By fixing the vibrational transition origin at the observed value, the observed transition frequencies were reproduced with the accuracy of about 0.02 cm^{-1} for both the ^{4}He–N_2O and ^{3}He–N_2O complexes, and the simulated infrared spectra were in consistent with the experimental spectra. Song *et al.* [45] further constructed another CCSD(T) IPES for the He–N_2O complex using a relatively larger basis set and the calculated rotational transition frequencies agree well with their recorded microwave spectra.

In general, the rigid N_2O model is believed to be sufficient to study the microwave spectra but could cause larger discrepancies for infrared spectra. Recently, we [70] have involved the dependence of the Q_3 normal mode for the v_3 antisymmetric stretching vibration of the N_2O molecule in the PES of He–N_2O and employed the three-dimensional DVR method to calculate the rovibrational states without separating the inter- and intramolecular nuclear motions. Figure 2 displays three counter plots of the CCSD(T) PES for He–N_2O. One can see that the IPES at each fixed Q_3 point gives a T-shaped global minimum and a linear local minimum at $\theta = 0^\circ$. For positive Q_3 values, the IPES has an additional small local minimum at $\theta = 180^\circ$. The global minimum of the He–N_2O complex on the three-dimensional PES was found to be a T-shaped structure at $R = 5.605$ a_0 and $\theta = 87.40^\circ$ with a well depth of 62.34 cm^{-1}. It is clear that the potential has a large angular anisotropy and strong radial–angular coupling.

The calculated pure vibrational bound states of ^{4}He–N_2O on this three-dimensional PES are given in table 2 together with the results on other two-dimensional PESs. In this table, n_s and n_b are respectively the vdW stretching and bending vibrational quantum numbers, which can only be loosely assigned due to significant mixing between the two vibrational modes. All the *ab initio* PESs support five vibrational bound states for ^{4}He–N_2O. The energy levels calculated from the SAPT PES [43] are lower than others because of its deeper potential well. The calculated vdW excited

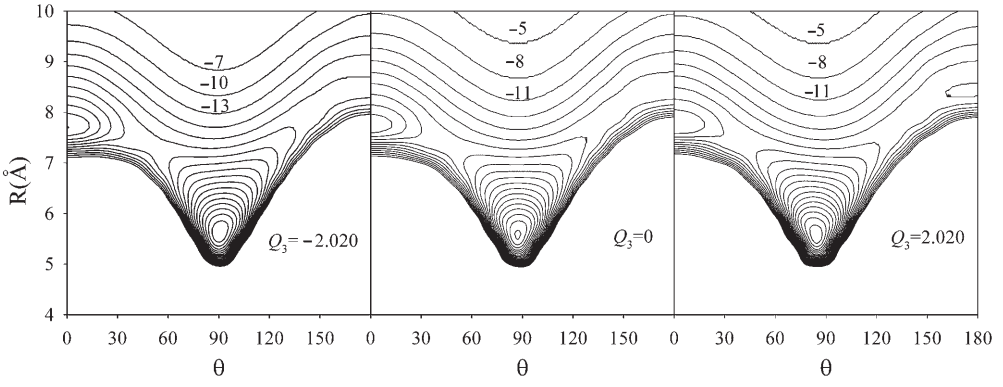

Figure 2. Contour plots of the CCSD(T) potential energy surfaces of He–N_2O for dimensionless $Q_3 = -2.020$, 0.0, and 2.020. Contours are labelled in cm^{-1}.

Table 2. Energy levels of the vibrational bound states for ^{4}He–N_2O. The energies for the v_3 state are relative to the v_3 fundamental frequency of the isolated N_2O molecule.

	Ground state				v_3 state
(n_s, n_b)	SAPT [43]	CCSD(T)[45]	CCSD(T)[44]	3D[70]	3D[70]
(0, 0)	−23.77	−21.3486	−19.9172	−21.4252	−21.2548
(0, 1)	−11.45	−9.3578	−8.9730	−9.3540	−9.3467
(0, 2)	−8.83	−7.2259	−6.8669	−7.2367	−7.2031
(0, 3)	−5.80	−4.1198	−3.6947	−4.1228	−4.0833
(1, 0)	−3.32	−2.1734	−1.7282	−2.2008	−2.1451

vibrational energy levels at the v_3 state of N_2O are very similar to those at its ground state. The predicted shift of the band origin for the ground vdW vibrational state from our three-dimensional PES was found to be 0.1704 and 0.1551 cm^{-1} for ^{4}He–N_2O and ^{3}He–N_2O respectively, which agrees well with the observed values of 0.2532 and 0.2170 cm^{-1} [137]. Figure 3 shows the contour plots of the wavefunctions for the vibrational states (0, 0), (0, 1), (0, 2), and (1, 0) of ^{4}He–N_2O. While the ground state is localized in the global minimum, the first excited state (0, 1) that corresponds to the first excitation in the bending coordinate is distributed over the global and the second minima, and the higher excited states are distributed more widely. The three lowest excited states are predominantly bending vibrations. The wavefunction for the first excited stretching vibrational state (1, 0) also shows some bending characters, due to strong radial–angular coupling.

We have also calculated the rovibrational energies of He–N_2O for J from 0 to 3 and $v = 0$ and 1 for the ground vdW vibrational state on the three-dimensional PES. The calculated relative line intensities of the rotational transitions in the v_3 region of N_2O were simulated at an estimated rotational temperature of $T = 2$ K. A portion of the calculated infrared spectra of He–N_2O are displayed in figure 4 together with the observed spectra [137]. The strongest transition is 1_{11}–0_{00} for ^{4}He–N_2O and 1_{01}–0_{00} for ^{3}He–N_2O. Significant isotopic effect was identified for the He atom, consistent with

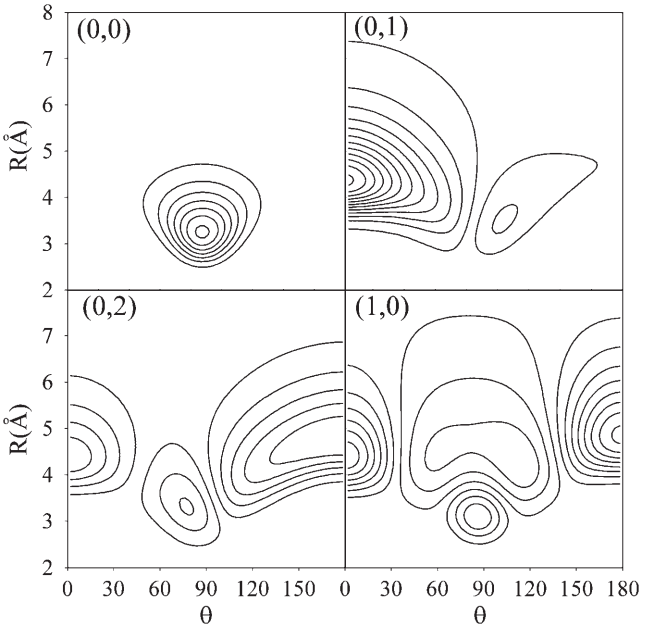

Figure 3. Contour plots of the wavefunctions for the vibrational states (0, 0), (0, 1), (0, 2), and (1, 0) of ^{4}He–N_2O.

the observed spectra. While the *a*-type transitions and *b*-type transitions are both prominent in ^{4}He–N_2O, the *b*-type transitions are very weak in ^{3}He–N_2O. The good agreement between the calculated and observed transition frequencies and relative intensities highlights the high quality of the three-dimensional PES.

3. H_2–(linear molecule) vdW complexes

Recently, vdW complexes containing H_2 have become an active topic of both experimental and theoretical studies. Different isotopomers of H_2 exhibit different quantum behaviours in various vdW complexes. Among the five familiar isotopomers of the hydrogen molecule (i.e., *para*H_2, *ortho*H_2, *para*D_2, *ortho*D_2, and HD), *para*H_2 and *ortho*D_2 have only even rotational angular momentum j_H, while *ortho*H_2 and *para*D_2 have only odd values of j_H. Because of the wide separation of rotational energy levels, at low temperature, *para*H_2 and *ortho*D_2 are at the $j_H = 0$ state, while *ortho*H_2 and *para*D_2 are at the $j_H = 1$ state. Among the H_2–(linear molecule) vdW complexes, H_2–HF is an early complex for which the *ab inito* four-dimensional PES and spectra were studied with the rigid monomer model [141, 142]. Recently, the vdW complexes containing a member of 'CO_2' family has been a considerable active subject of research. OCS, N_2O and CO_2 are the members of this family. Each molecule of the family has a strong infrared fundamental stretching vibration and displays similar spectroscopic behaviours. The infrared spectra of several dimers [143–146] and clusters [147–160] of this family

with H_2 have been observed in the region of the ν_3 band of the linear molecule OCS, N_2O, or CO_2. In order to fully predict the infrared spectra, five-dimensional PESs for the H_2–OCS [13], H_2–N_2O [161], and H_2–CO_2 [162] systems that include explicit dependence on the Q_3 normal vibration of the monomer molecule were constructed. In our studies [161, 162], the radial discrete variable representation/angular finite basis representation (radial DVR/angular FBR) method was applied to calculate the rovibrational states without separating the inter- and intramolecular nuclear motions. Although the approach (described below) is focused on the H_2–(linear molecule) complexes, it can be straightforwardly extended to any (linear molecule) dimers in which one of the linear molecules can be assumed as a rigid rotor.

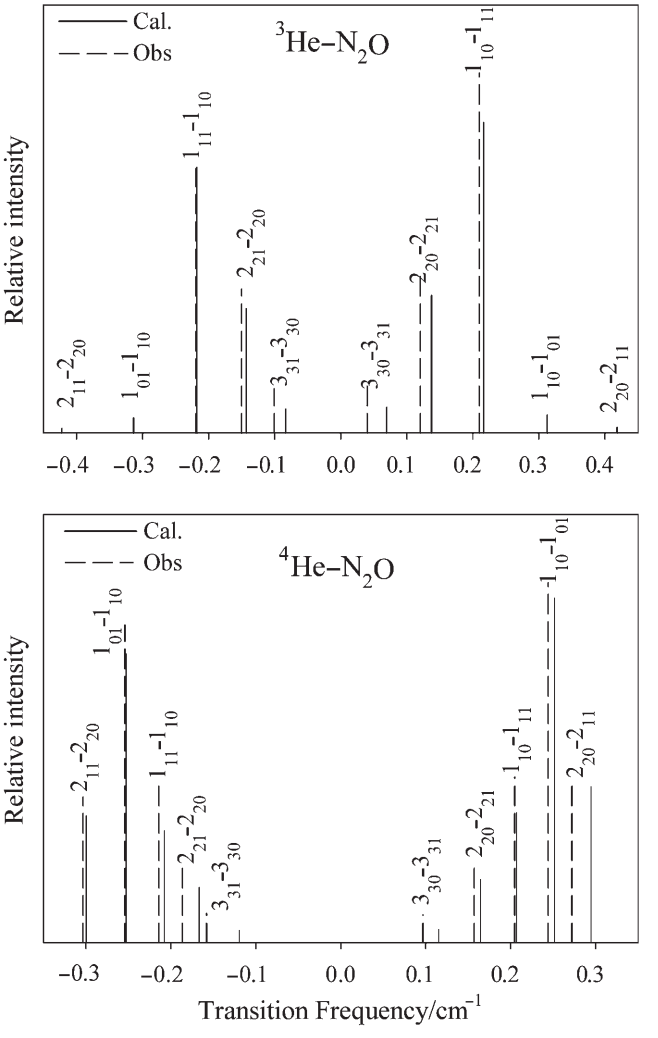

Figure 4. Calculated [44] and observed [137] line intensities for ^{3}He–N_2O and ^{4}He–N_2O. The transition frequencies are relative to the band origin.

3.1. *Hamiltonian without separating the inter- and intramolecular vibrations*

In general, the geometry of the H_2–(linear molecule) complex can be described in the Jacobi coordinates $(R, r_1, \varphi, \theta_1, \theta_2, Q)$ [163], as shown in figure 5. R denotes the separation between the H_2 centre of mass and the centre of mass of the linear molecule. Q is the normal mode for the intramolecular vibration responsible for the infrared spectra. r_1 is the bond length of the H_2 molecule, which can be treated as a rigid rotor, since the vibrational state of H_2 has not been changed in the observed infrared spectra. The bond length of the H_2 molecule can be taken as the observed averaged value at its ground vibrational state, $\langle r_1 \rangle_0 = 0.7666$ Å [10]. The angle between the vector $\boldsymbol{R}$ and H_2 (or the linear molecule) is defined as θ_1 (or θ_2). φ denotes the dihedral angle between the two half-planes extending from the vector $\boldsymbol{R}$ to one H atom (labelled as H1 in figure 5) and one end of the linear molecule. Without separating the inter- and intramolecular vibrations, the rovibrational Hamiltonian of the H_2–(linear molecule) complex can be written as [1,164] (in atomic units)

$$\hat{H} = -\frac{1}{2\mu_1}\frac{\partial^2}{\partial R^2} - \frac{1}{2\mu_2}\frac{\partial^2}{\partial Q^2} + B_1\hat{\boldsymbol{j}}_1^2 + \frac{\hat{\boldsymbol{j}}_2^2}{2I_Q} + \frac{(\hat{\boldsymbol{J}} - \hat{\boldsymbol{j}}_1 - \hat{\boldsymbol{j}}_2)^2}{2\mu_1 R^2} + V(R, \varphi, \theta_1, \theta_2, Q) \qquad (22)$$

where μ_1 is the reduced mass of the H_2–(linear molecule) dimer, and μ_2 is the effective reduced mass for the coordinate Q of the linear molecule. I_Q is the rotational moment of

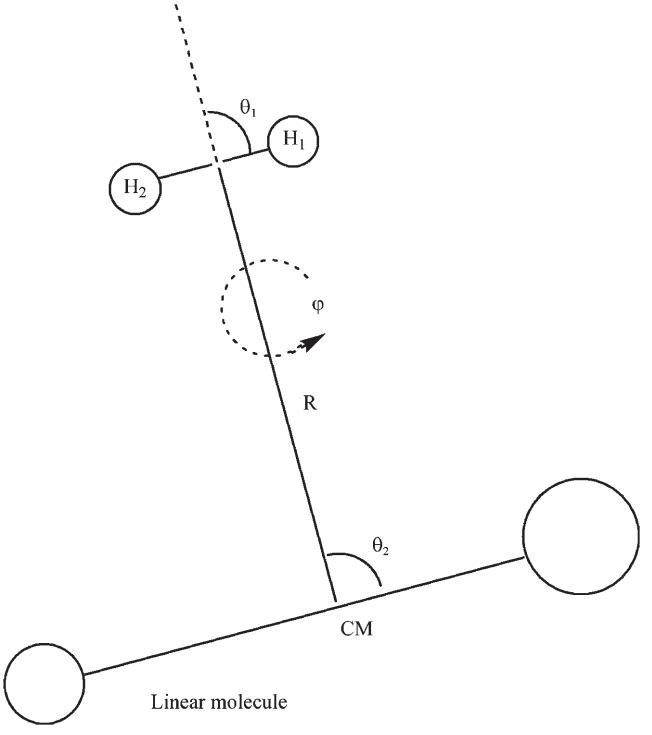

Figure 5. Jacobi coordinates for the H_2–(linear molecule) complex.

inertia of the linear molecule and varies with Q. B_1 represents the rotational constant of the H_2 isotopomer, which is taken as the observed value of $59.3220\,cm^{-1}$ for H_2 and $29.9037\,cm^{-1}$ for D_2, as adopted in [13]. $\hat{\boldsymbol{J}}$, $\hat{\boldsymbol{j}}_1$ and $\hat{\boldsymbol{j}}_2$ are the angular momentum operators corresponding to the total and monomer rotations. V is the total potential energy of the complex and could be divided into two terms,

$$V(R, \varphi, \theta_1, \theta_2, Q) = V_1(Q) + \Delta V(R, \varphi, \theta_1, \theta_2, Q), \tag{23}$$

where $\Delta V(R, \varphi, \theta_1, \theta_1, Q)$ is the IPES between the linear molecule and the H_2 molecule.

The efficient radial DVR/angular FBR method [165, 166] can be employed to represent the rovibrational Hamiltonian. The vibrational motion for the coordinate R is represented by sine-DVR [72] and that for the coordinate Q is represented by PODVR [71, 73]. For the angular part, one can use the FBR method with the parity-adapted BF basis of the following form [167–169],

$$\begin{aligned}\left|j_1 j_2 mK; JMp\right\rangle = (2 + 2\delta_{K,0}\delta_{m,0})^{-1/2}[&D^{J*}_{MK}(\alpha,\ \beta,\ \gamma) Y_{j_1 m}(\theta_1, \phi)\Theta_{j_2 K-m}(\theta_2) \\ &+ (-1)^{J+p} D^{J*}_{M-K}(\alpha,\ \beta,\ \gamma) Y_{j_1 -m}(\theta_1, \phi)\Theta_{j_2 m-K}(\theta_2)],\end{aligned} \tag{24}$$

where D^J_{MK}, $Y_{j,m}$, and $\Theta_{j_2 K-m}$ are the normalized rotational functions, spherical harmonic functions, and associated Legendre polynomials, respectively. In the FBR, the matrix elements of the first two angular kinetic energy operators in equation (22) are diagonal. The third angular kinetic energy operators is calculated as follows,

$$\begin{aligned}&\left\langle j_1', j_2', m', K'; JMp\right|(\hat{\boldsymbol{J}} - \hat{\boldsymbol{j}}_1 - \hat{\boldsymbol{j}}_2)^2 \left|j_1, j_2, m, K; JMp\right\rangle \\ &= \left\langle j_1', j_2', m', K'; JMp\right|\hat{J}^2 - \hat{\boldsymbol{J}}(\hat{\boldsymbol{j}}_1 + \hat{\boldsymbol{j}}_2) - (\hat{\boldsymbol{j}}_1 + \hat{\boldsymbol{j}}_2)\hat{\boldsymbol{J}} + (\hat{\boldsymbol{j}}_1 + \hat{\boldsymbol{j}}_2)^2\left|j_1, j_2, m, K; JMp\right\rangle \\ &= [J(J+1) - 2K^2 + 2m(K-m) + j_1(j_1+1) + j_2(j_2+1)]\delta(j_1' j_1)\delta(j_2' j_2)\delta(K', K)\delta(m', m) \\ &\quad - (1 + \delta(K', 0)\delta(m', 0))^{1/2}\Lambda^-_{JK}\Lambda^-_{j_1 m}\delta(j_1' j_1)\delta(j_2' j_2)\delta(K', K-1)\delta(m', m-1) \\ &\quad - (1 + \delta(K, 0)\delta(m, 0))^{1/2}\Lambda^+_{JK}\Lambda^+_{j_1 m}\delta(j_1' j_1)\delta(j_2' j_2)\delta(K', K+1)\delta(m', m+1) \\ &\quad - (1 + \delta(K', 0)\delta(m, 0))^{1/2}\Lambda^-_{JK}\Lambda^-_{j_2 K-m}\delta(j_1' j_1)\delta(j_2' j_2)\delta(K', K-1)\delta(m', m) \\ &\quad - (1 + \delta(K, 0)\delta(m, 0))^{1/2}\Lambda^+_{JK}\Lambda^+_{j_2 K-m}\delta(j_1' j_1)\delta(j_2' j_2)\delta(K', K+1)\delta(m', m) \\ &\quad + (1 + \delta(K, 0)\delta(m, 0))^{1/2}\Lambda^+_{j_1 m}\Lambda^-_{j_2 K-m}\delta(j_1' j_1)\delta(j_2' j_2)\delta(K', K)\delta(m', m+1) \\ &\quad + (1 + \delta(K, 0)\delta(m', 0))^{1/2}\Lambda^-_{j_1 m}\Lambda^+_{j_2 K-m}\delta(j_1' j_1)\delta(j_2' j_2)\delta(K', K)\delta(m', m-1)\end{aligned} \tag{25}$$

The matrix elements of the potential could be calculated conveniently in grid representation in which the potential energy matrix is diagonal. The transformation between the FBR and DVR for the angular variables could be easily carried out [170]. The Lanczos method can be employed to efficiently diagonalize the Hamiltonian matrix to produce the energy levels and wavefunctions of the rovibrational states.

3.2. *Hamiltonian with separating the inter- and intramolecular vibrations*

The above approach contains full coupling between the inter- and intramolecular vibrations. Due to high rovibrational energy levels in the region of the vibrational excited state of the linear molecule, the convergence of those levels needs a very long Lanczos propagation. Such calculations are affordable for the Rg–(linear molecule) complexes, but become very difficult and time-consuming for the H_2–(linear molecule) complexes. It is thus highly desirable to separate the inter- and intramolecular vibrations if feasible. Since the intramolecular vibrational mode has much higher frequency than the intermolecular mode in weakly bounded vdW complexes, it is indeed possible to separate the inter- and intramolecular vibrations if the off-diagonal vibrational coupling is sufficiently small. In this approximation, the total rovibrational wavefunction is assumed to have the following direct product form,

$$\Psi_{nv}^{JMp}(R,\varphi,\theta_1,\theta_2,Q,\alpha,\beta,\gamma) = \Phi_{nv}^{JMp}(R,\varphi,\theta_1,\theta_2,\alpha,\beta,\gamma)\psi_v(Q), \tag{26}$$

where v is the quantum number for a specific vibrational state of the linear molecule, and $\psi_v(Q)$ are the corresponding vibrational wavefunctions, defined in equation (5). In particular, one can focus on the ground ($v=0$) and the first excited ($v=1$) vibrational states of the linear molecule only, which are adequate to make the full comparison with the observed infrared spectra possible. Using equation (26), one can conveniently define the four-dimensional vibrationally averaged intermolecular PES $V_v(R, \varphi, \theta_1, \theta_2)$ as [65]

$$V_v(R,\varphi,\theta_1,\theta_2) = \int_{-\infty}^{\infty} \psi_v(Q)\Delta V(R,\varphi,\theta_1,\theta_2,Q)\psi_v(Q)\mathrm{d}Q, \tag{27}$$

and the vibrationally averaged intermolecular Hamiltonian,

$$\hat{H}_v = -\frac{1}{2\mu_1}\frac{\partial^2}{\partial R^2} + B_1\hat{\boldsymbol{J}}_1^2 + B_v\hat{\boldsymbol{J}}_2^2 + \frac{(\hat{\boldsymbol{J}}-\hat{\boldsymbol{j}}_1-\hat{\boldsymbol{J}}_2)}{2\mu_1 R^2} + V_v(R,\varphi,\theta_1,\theta_2) \tag{28}$$

where, $B_v = \langle\psi_v|(2I_Q)^{-1}|\psi_v\rangle$. On use of the PODVR, the averaged potential can be easily calculated as

$$V_v(R,\varphi,\theta_1,\theta_2) = \sum_k T_{kv}^2 \Delta V(R,\varphi,\theta_1,\theta_2,Q_k), \tag{29}$$

where T is the transformation matrix between the FBR and PODVR, $T_{kv} = \sqrt{\omega_k}\psi_v(Q_k)$ where the ω_k are the weights at the PODVR grid point Q_k. The above summation can be directly performed upon the *ab initio* points so that the fitting of the potential in the coordinate Q is not needed. The averaged potentials $V_v(R, \varphi, \theta_1, \theta_2)$ are very useful for the simulation of vdW clusters [171, 172]. This approximation of separating the inter- and intramolecular vibrations by averaging the Hamitonian with the vibrational wavefunction of the linear molecule is superior to the rigid monomer model for the

diagonal coupling between the inter- and intramolecular vibrations is included in this approximation.

3.3. *Fitting of the potential energy surface and dipole moment surfaces*

The calculated *ab initio* intermolecular potential energies $\Delta V(R, \varphi, \theta_1, \theta_2, Q)$ for each pair of R and Q values could be fitted to the following analytical form [173] in the angular variables,

$$\Delta V(R,\varphi,\theta_1,\theta_2,Q) = \left[\sum_{l_1 l_2 l} g_{l_1 l_2 l}(R,Q) A_{l_1 l_2 l}(\theta_1,\theta_2,\varphi)\right] \exp\left[\sum_{l_1 l_2 l} d_{l_1 l_2 l}(R,Q) A_{l_1 l_2 l}(\theta_1,\theta_2,\varphi)\right] \tag{30}$$

with

$$A_{l_1 l_2 l}(\theta_1,\theta_2,\varphi) = \sum_{m=-l_<}^{l_<} \begin{pmatrix} l_1 & l_2 & l \\ m & -m & 0 \end{pmatrix} Y_{l_1 m}(\theta_1,\varphi_1) Y_{l_2,-m}(\theta_2,\varphi_2) \tag{31}$$

where $\varphi = \varphi_1 - \varphi_2$ and $l_< = \min(l_1, l_2)$. l is the vector sum of l_1 and l_2, and the three indices satisfy the restrictions that both l_1 and $l+l_1+l_2$ must be even because of the symmetric properties of the H_2 molecule and the invariance of the potential with respect to the reflection in the plane containing the z axis and the linear molecule. The potentials for each pair of R and Q values are fitted separately, and the potential energy for any arbitrary R can be obtained by a cubic spline interpolation.

In order to calculate the line intensities, the dipole moments of the complex in the BF frame need to be calculated. For each pair of the R and Q values, the components of the dipole moments are fitted to the following analytic functions [1],

$$\mu_\alpha(R,\varphi,\theta_1,\theta_2,Q) = \sum_{l_1 l_2 l} g_{l_1 l_2 l;\alpha}(R,Q) A_{l_1 l_2 l;\alpha}(\theta_1,\theta_2,\varphi), \quad \alpha = x, y, \quad \text{or } z. \tag{32}$$

For μ_z, the angular form is just the same as that for the potential energy. For μ_x and μ_y, the angular forms are taken as

$$A_{l_1 l_2 l;x}(\theta_1,\theta_2,\varphi) = \sum_m \begin{pmatrix} l_1 & l_2 & l \\ m & -m+1 & -1 \end{pmatrix} \Theta_{l_1 m}(\theta_1) \Theta_{l_2 -m+1}(\theta_2) \cos(m\varphi), \tag{33}$$

$$A_{l_1 l_2 l;y}(\theta_1,\theta_2,\varphi) = \sum_m \begin{pmatrix} l_1 & l_2 & l \\ m & -m+1 & -1 \end{pmatrix} \Theta_{l_1 m}(\theta_1) \Theta_{l_2 -m+1}(\theta_2) \sin(m\varphi), \tag{34}$$

respectively. The above forms satisfy the symmetric properties of the dipole moments of the complex. The dipole moments for any R can be obtained by a cubic spline interpolation.

3.4. *Calculation of the transition intensities*

In the FBR, the total rovibrational wavefunction for a rovibrational state n can be rewritten as:

$$\Psi_n^{JMp}(R,\varphi,\theta_1,\theta_2,Q,\alpha,\beta,\gamma)=\sum_{j_1,j_2,m,K,v_1,v_2} c^{nJp}_{j_1,j_2,m,K,v_1,v_2}\varphi_{v_1}(R)\varphi_{v_2}(Q)\big|j_1j_2mK;JMp\big\rangle. \quad (35)$$

In order to calculate the line intensity, the above equation is rewritten as

$$\Psi_n^{JMp}(R,\varphi,\theta_1,\theta_2,Q,\alpha,\beta,\gamma)=\sum_K\Big[\Psi^{Jnp}_{K+}(R,\varphi,\theta_1,\theta_2,Q)D^{J*}_{MK}(\alpha,\beta,\gamma) + (-1)^{J+p}\Psi^{Jnp}_{K-}(R,\varphi,\theta_1,\theta_2,Q)D^{J*}_{M-K}(\alpha,\beta,\gamma)\Big] \quad (36)$$

where

$$\Psi^{Jnp}_{K+}(R,\varphi,\theta_1,\theta_2,Q)= \sum_{j_1,j_2,m,v_1,v_2}(2+2\delta_{K,0}\delta_{m,0})^{-1/2}c^{nJp}_{j_1,j_2,m,K,v_1,v_2}\varphi_{v_1}(R)\varphi_{v_2}(Q)Y_{j_1m}(\theta_1,\phi)\Theta_{j_2K-m}(\theta_2) \quad (37)$$

and

$$\Psi^{Jnp}_{K-}(R,\varphi,\theta_1,\theta_2,Q)= \sum_{j_1,j_2,m,v_1,v_2}(2+2\delta_{K,0}\delta_{m,0})^{-1/2}c^{nJp}_{j_1,j_2,m,K,v_1,v_2}\varphi_{v_1}(R)\varphi_{v_2}(Q)Y_{j_1-m}(\theta_1,\phi)\Theta_{j_2m-K}(\theta_2) \quad (38)$$

The line intensity of a transition from an initial rovibrational state $|Jpn\rangle$ to a final state $\big|J'p'n'\big\rangle$ at a temperature T can be calculated as,

$$\begin{aligned} I_{Jpn\to J'p'n'} \propto{}& (2J+1)(2J'+1)(E_{J'p'n'}-E_{Jpn})[e^{-E_{Jpn}/kT}-e^{-E_{J'p'n'}/kT}] \\ &\Bigg|\sum_K\sum_{K'}\sum_h(-1)^K\Bigg\{\begin{pmatrix} J & J' & 1\\ -K & K' & h\end{pmatrix}\int\Psi^{Jnp^*}_{K+}\mu_h\Psi^{J'n'p'}_{K'+}\,d\tau \\ &+(-1)^{J+p}\begin{pmatrix} J & J' & 1\\ K & K' & h\end{pmatrix}\int\Psi^{Jnp^*}_{K-}\mu_h\Psi^{J'n'p'}_{K'+}\,d\tau \\ &+(-1)^{J'+p'}\begin{pmatrix} J & J' & 1\\ -K & -K' & h\end{pmatrix}\int\Psi^{Jnp^*}_{K+}\mu_h\Psi^{J'n'p'}_{K'-}\,d\tau \\ &+(-1)^{J+p+J'+p'}\begin{pmatrix} J & J' & 1\\ K & -K' & h\end{pmatrix}\int\Psi^{Jnp^*}_{K-}\mu_h\Psi^{J'n'p'}_{K'-}\,d\tau\Bigg\}\Bigg|^2 \end{aligned} \quad (39)$$

The integrals in equation (39) can be conveniently evaluated in the DVR. In the approximation of separating the inter- and intramolecular vibrations, the calculations of the transition intensities require the transition dipole moments from the ground ($v=0$) to the first excited ($v=1$) vibrational state of the linear molecule, which can be evaluated as

$$\bar{\mu}_\alpha(R,\varphi,\theta_1,\theta_2)=\int_{-\infty}^{\infty}\psi_{v=1}(Q)\mu_\alpha(R,\varphi,\theta_1,\theta_2,Q)\psi_{v=0}(Q)\mathrm{d}Q. \tag{40}$$

In the PODVR, the above integral is expressed as,

$$\bar{\mu}_\alpha(R,\varphi,\theta_1,\theta_2)=\sum_k T_{k1}\mu_\alpha(R,\varphi,\theta_1,\theta_2,Q)T_{k0}. \tag{41}$$

The four-dimensional averaged potential (equation 29) and the transition dipole moment surface (equation 41), summed over the PODVR grid points of Q, can be directly calculated upon the *ab initio* points and then fitted by use of equations (30) and (32). It is clear that the fittings of the PES and dipole moment surfaces in the intramolecular coordinate Q can be avoided in this way. For a symmetrical linear molecule such as CO_2, $\psi_{v=1}(Q)$ is zero for $Q=0$, so that the dipole moments at $Q=0$ make no contributions to the transition dipole moments (see equation 40). As a result, the rigid monomer model could produce qualitatively correct transition intensities in the infrared spectra related to the one-quantum antisymmetric vibrational transition of the symmetrical linear molecule only if the appropriate transition dipole functions, defined in equation (40), are used.

3.5. *H_2–N_2O*

In 2002, Tang and McKellar [144] have studied the infrared spectra of five H_2–N_2O complexes in the region of the ν_3 fundamental band of N_2O. The observed bands were predominantly *a*-type plus some weak *b*-type transitions in the case of D_2–N_2O. The band origins for all the five complexes were found to be blue-shifted, and obvious regularities were detected. The $j_H=1$ forms have larger shifts than their $j_H=0$ counterparts, and the shifts increase from H_2 to HD to D_2. The same regularity was also found in the H_2–OCS complexes [143]. About three years later, the high-resolution infrared spectra of complexes containing the H_2 clusters and N_2O were recorded in the ν_3 region of N_2O [158]. Clusters with the size up to $n=13$ for $(para H_2)_n$ –N_2O and $n=7$ for $(ortho H_2)_n$ –N_2O were analysed. Besides the observed *P*- and *R*-branch lines, the *para*H_2 clusters have no prominent *Q*-branch features, probably due to the fact that most of them are in the $K=0$ levels, for which *Q*-branches are forbidden. Nevertheless, strong *Q* features were observed in the *ortho*H_2 spectra due to an opposite spin symmetry. The derived vibrational band origins began to shift to blue at $n=5$ or 6, and no obvious superfluid effects were indicated for $(para H_2)_n$–N_2O clusters up to $n=13$.

We [161] have studied the PES and infrared spectra of the H_2–N_2O complexes by including the Q_3 normal mode of the N_2O molecule in the calculations of the potential

energies and the bound states. The global minimum of the complex has a depth of 242.43 cm^{-1} at $Q_3 = 0$, $R = 5.43$ a_0, $\theta_1 = 91.9°$ and $\theta_2 = 94.6°$ for a planar geometry. Figures 6(a) and (b) show the corresponding contour plots of the potential energy surface as a function of θ_1 and θ_2 at $Q_3 = -0.5246$, $R = 5.43$ a_0, $\varphi = 0$ and 90 respectively. One can see that the global minimum region is rather narrow in the angle θ_2 while it is much broader in the coordinate θ_1. The minimum at $\varphi = 90$ is turned out to be a saddle point along the dihedral coordinate φ. Figure 6(c) shows the contour plot of the PES as a function of θ_1 and φ at $Q_3 = -0.5246$, $R = 5.43$ a_0, and $\theta_2 = 93.6°$. This figure is very smooth, which shows that the potential energy varies slightly along the coordinates θ_1 and φ.

The rovibrational energy levels for the H_2–N_2O complexes were calculated using the five-dimensional radial DVR/angular FBR method and Lanczos algorithm without separating the inter- and intramolecular vibrations. Table 3 gives the energy levels for the first ten pure vibrational bound states of the H_2–N_2O complexes. Due to the large separation of the rotational energy levels for the H_2 molecule, the rotational states of *para*H_2 and *ortho*D_2 are set to the $j_1 = 0$ state of the free hydrogen monomer, while that of *ortho*H_2 and *para*D_2 at $j_1 = 1$, although j_1 is not a good quantum number in the complex. The five-dimensional PES supports 8, 16, 14, and 26 bound states with $J = 0$

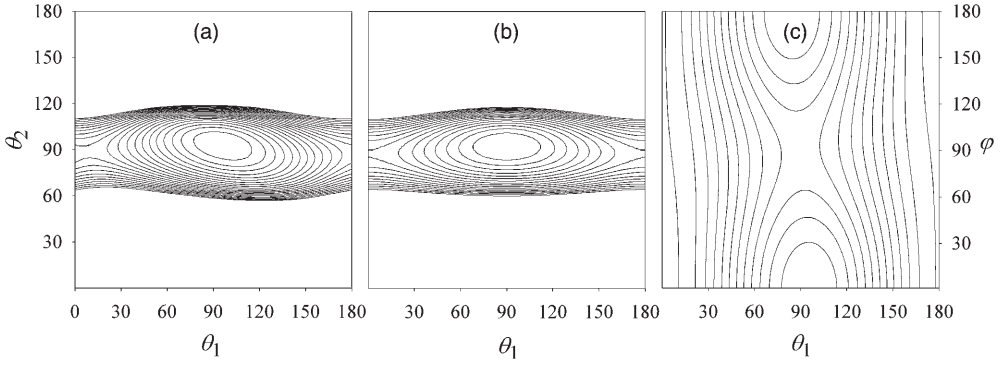

Figure 6. Contour plots of the potential energy surface of H_2–N_2O for $Q_3 = -0.5246$. (a) $R = 5.43$ a_0 and $\phi = 0$. (b) $R = 5.43$ a_0 and $\phi = 90$. (c) $R = 5.43$ a_0 and $\theta_2 = 93.6$. The contour spacing is 30 cm^{-1}.

Table 3. Pure vibrational energy levels (in cm^{-1}) for the first ten bound states of four species of H_2–N_2O.

n	*para*H_2–N_2O	*ortho*H_2–N_2O	*ortho*D_2–N_2O	*para*D_2–N_2O
1	−64.72	−87.02	−84.62	−107.92
2	−35.05	−55.25	−52.95	−74.44
3	−27.61	−41.08	−40.62	−56.86
4	−23.32	−36.71	−36.46	−50.98
5	−18.16	−31.94	−30.28	−46.80
6	−11.04	−29.85	−28.04	−45.01
7	−6.74	−27.24	−23.26	−43.10
8	−0.93	−21.96	−17.80	−38.73
9		−17.28	−13.65	−35.65
10		−12.69	−8.56	−29.94

Table 4. Comparison of the observed [144] and calculated [161] shifts (in cm^{-1}) of the band origin for the species of H_2–N_2O complexes relative to the free N_2O molecule.

Species	Obs	Cal.
paraH_2–N_2O	0.2261	0.2219
orthoH_2–N_2O	0.6238	0.4236
orthoD_2–N_2O	0.4534	0.3585
paraD_2–N_2O	0.7900	0.5437
HD–N_2O	0.3180	

for *para*H_2–, *ortho*H_2–, *para*D_2–, and *ortho*D_2–N_2O, respectively. By analysing the wavefunctions of the vibrational bound states, it was found that the ground vibrational state is localized at the global minimum and the first excited state corresponds to the vdW bending vibration for all the four species. For D_2–N_2O, the second excited state has significant vdW stretching character, whereas the higher excited states show a strong mixing between the bending and stretching vibration modes. For H_2–N_2O, all the excited states are characterized as the overtone bending vibrations. The calculated band shifts for the ν_3 vibrational state of N_2O are given in table 4 together with the observed values. All the calculated band origins are blue-shifted, and reproduce the experimental values well, especially for the *para*H_2–N_2O complex.

We have also calculated the frequencies and the corresponding intensities in the ν_3 range of N_2O to compare with the observed infrared spectra. The calculated relative line intensities of the rotational transitions in the ν_3 region of N_2O for the vdW ground vibrational state were simulated at an estimated rotational temperature of $T = 1.5\,K$. The calculated infrared spectra of the H_2–N_2O complexes are displayed in figure 7 together with the observed spectra [144]. The calculated spectra are in good agreement with the observed spectra, especially for the *para*H_2–N_2O complex. The calculated transition frequencies agree very well with the observed values with a rms error of about $0.02\,cm^{-1}$ for the H_2–N_2O complexes and $0.04\,cm^{-1}$ for the D_2–N_2O complexes. Moreover, significant isotopic effect was found for the H atom. The spectra contain only *a*-type transitions for the H_2–N_2O complexes, while for the D_2–N_2O complexes, both the parallel band ($\Delta K_a = 0$) and perpendicular band ($\Delta K_a = \pm 1$) are prominent, and even some *a*-type transitions with ($\Delta K_a = \pm 2$) have significant line strengths.

3.6. *H_2–CO_2*

The infrared spectra of H_2–CO_2 were less studied among all vdW complexes containing the CO_2 family. This is partially because half of the rotational levels are missing due to the nuclear-spin symmetry of the CO_2 molecule so that only fewer transitions can be observed. McKellar [145] has presented its infrared spectra in the region of the CO_2 ν_3 antisymmetric stretching vibration using a tunable diode laser probe and a pulsed supersonic jet expansion. It was demonstrated that *ortho*H_2 complexes bind more strongly than the *para*H_2 ones and tend to dominate in the cold dynamic jet environment as other vdW complexes containing hydrogen, like H_2–N_2O and H_2–OCS. The three *para*H_2 isotopic species (H_2–$^{12}C^{16}O_2$, H_2–$^{13}C^{16}O_2$, and H_2–$^{12}C^{18}O_2$) have T-shaped structures with intermolecular distance of about 3.5 Å,

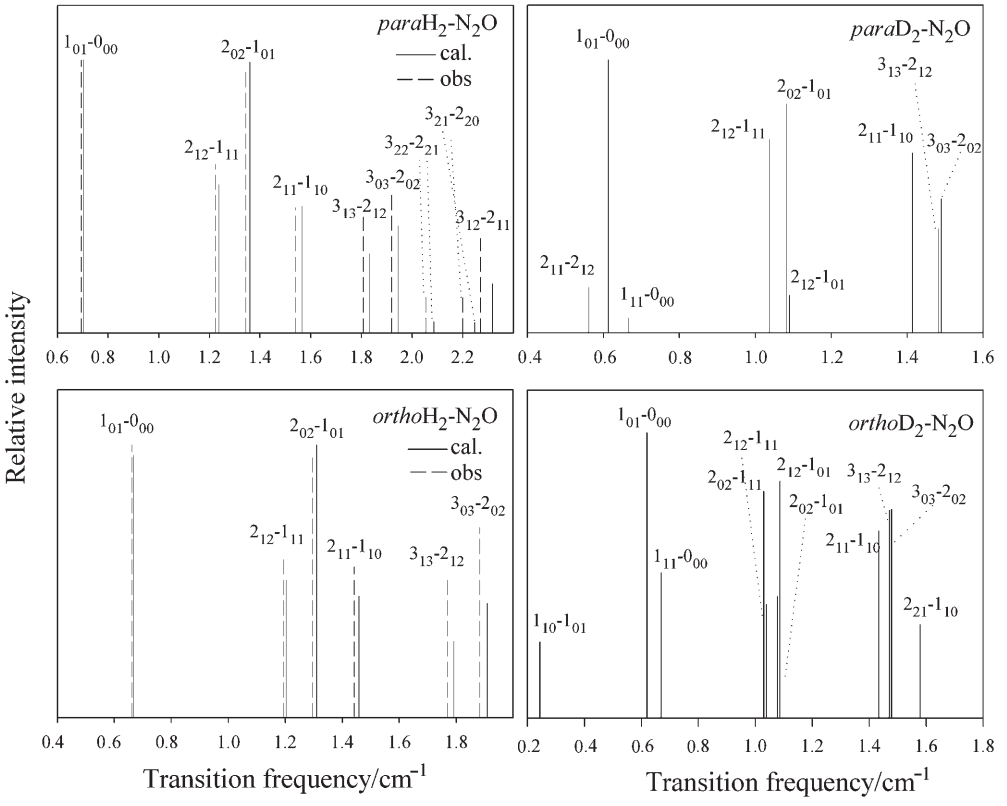

Figure 7. Calculated [161] and observed [144] line intensities for the H_2–N_2O complexes. The transition frequencies are relative to the band origin.

and have very similar band origin shifts of about $-0.2\,cm^{-1}$. Due to the interchange symmetry of the indistinguishable O nuclei, only half of the rotational energy levels are allowed so that relatively few lines were observed and assigned for the *para*H_2 complexes. The spectra of *ortho*H_2–CO_2 were found to be more complicated and difficult to be assigned.

Wang *et al.* [174] have computed a four-dimensional *ab initio* PES for the H_2–CO_2 complex at the CCSD(T) level by fixing the geometry of H_2 and CO_2 at their vibrationally averaged values. The PES has a global minimum with a well depth of $211.9\,cm^{-1}$. It supports seven vibrational bound states for *para*H_2–CO_2 and 19 for *ortho*H_2–CO_2. The binding energy of *ortho*H_2–CO_2 is $71.7\,cm^{-1}$, which is significantly larger than that of *para*H_2–CO_2 ($50.4\,cm^{-1}$), indicating that the *ortho*H_2 complex is more stable. The normal isotope of CO_2 can only have even values of the angular momentum corresponding to its rotation in the vibrational ground state due to the interchange symmetry of the indistinguishable zero-spin ^{16}O nuclei. It was thus identified that the allowed rotational levels have $(K_a, K_c) = (\text{even, even})$ or (odd, odd) for *para*H_2–CO_2 as compared to (even, odd) or (odd, even) for *ortho*H_2–CO_2, which is the key to the assignment of the observed transitions for *ortho*H_2–CO_2 and revealed that *ortho*H_2 is perpendicular to the intermolecular axis in the complex. They further

Table 5. Comparison of the calculated pure vdW vibrational energy levels (in cm^{-1}) for the *para*H_2–CO_2 complex in both $\nu_3 = 0$ and 1 states of CO_2 with (E_1) and without (E_2) the inter- and intramolecular vibrational coupling.

	Ground state		Excited state	
(n_s, n_b)	E_1	E_2	E_1	E_2
(0, 0)	−54.408	−54.390	−54.514	−54.504
(0, 1)	−31.129	−31.118	−31.255	−31.248
(0, 2)	−25.533	−25.525	−25.656	−25.651
(0, 3)	−22.221	−22.214	−22.369	−22.365
(0, 4)	−17.245	−17.237	−17.382	−17.376
(0, 5)	−9.165	−9.157	−9.290	−9.285
(1, 0)	−5.057	−5.052	−5.135	−5.132
(0, 6)	−0.726	−0.722	−0.792	−0.790

calculated the transition frequencies in the infrared spectra region, which agree well with the observed results.

We [162] have recently constructed a five-dimensional potential energy surface that explicitly involves the dependence of the Q_3 normal mode of the CO_2 molecule by the supermolecular approach with the full counterpoise correction using the CCSD(T) method. Two equivalent global minima are located at $R = 2.97$ Å, $\theta_1 = 90°$, $\theta_2 = 90°$, $\varphi = 0$ or 180° with a well depth of 219.68 cm^{-1}. The saddle point connecting the two equivalent global minima is at $R = 3.10$ Å, $\theta_1 = 90°$, $\theta_2 = 90°$ and $\varphi = 90°$ with a barrier height of 82.41 cm^{-1}.

We have also calculated the pure vibrational energy levels for the H_2–CO_2 complexes using the five-dimensional radial DVR/angular FBR method and Lanczos algorithm without and with separating the inter- and intramolecular vibrations. Table 5 presents the comparison of the pure vdW vibrational levels for *para*H_2–CO_2 separately determined from the two approaches, and the differences for most of the calculated energy levels are within 0.01 cm^{-1}. Thus, the off-diagonal inter- and intramolecular vibrational coupling is proved to be very small in the case of H_2–CO_2, so that the separation including the diagonal coupling should be a good approximation with high accuracy. Our new PES supports 8, 22, 14 and 36 pure vibrational bound states for *para*H_2–, *ortho*H_2–, *ortho*D_2–, and *para*D_2–CO_2 respectively. The calculated zero point energies (ZPEs) for H_2–CO_2 complexes are very large, for example, the ZPE is 165.29 cm^{-1} for *para*H_2–CO_2 and 147.07 cm^{-1} for *ortho*D_2–CO_2, which are more than half of the global well depth. The large ZPE is mainly contributed from the H_2 hindered rotation in the complex, similar to the case of H_2–N_2O and H_2–OCS. Figure 8 shows the contour plots of probability densities for (R, θ_2) integrated over other variables for all the vibrational bound states of *para*H_2–CO_2. Since the complex has only one minimum for (R, θ_2), most of the vibrational bound states have clear nodal structures and could be easily assigned with the vdW stretching (n_s) and bending (n_b) quantum numbers. The seventh state corresponds to the first excited vdW stretching vibrational state with a minor bending character. The highest bound state (0, 6) is dominated by the bending vibration and has a small mixing of the stretching character. The calculated shift of the band origin for the ν_3 vibrational state of CO_2 was found to be −0.113, −0.099, −0.089, and −0.099 cm^{-1} for the *para*H_2–, *ortho*H_2–, *para*D_2–,

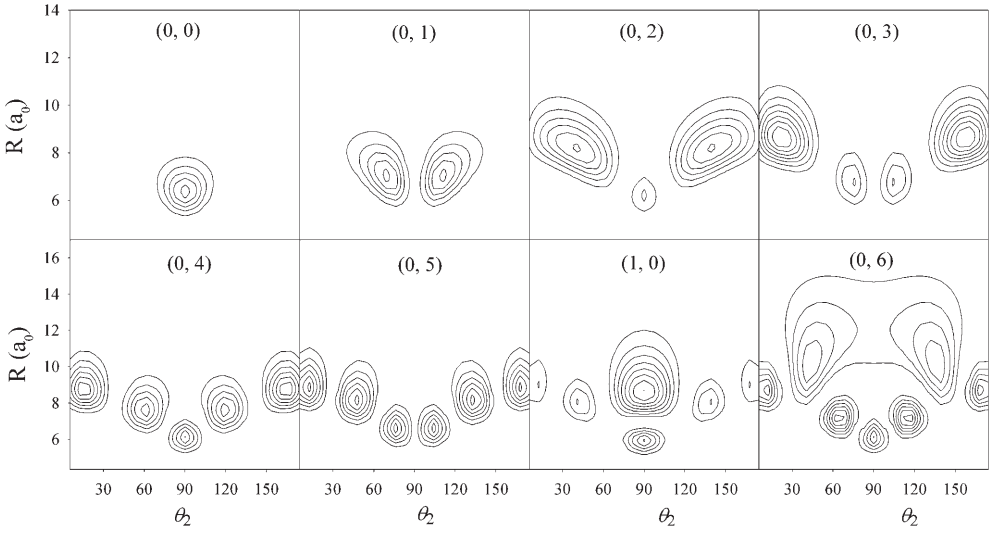

Figure 8. Contour plots of probability densities for all the vibrational bound states of *para*H_2–CO_2.

and *ortho*D_2–CO_2 complexes, respectively, the first two of which are in good agreement with the observed values of -0.198 and $-0.096\,cm^{-1}$.

The transition frequencies and the corresponding intensities in the v_3 range of CO_2 were also computed. It was found that the transitions from the $J=0$ state are not allowed for *ortho*H_2–CO_2 or *para*D_2–CO_2, because their ground vibrational states has odd symmetry for the exchange of two O atoms. Figure 9 plots the calculated [162] infrared spectra for *para*H_2–, *ortho*H_2–, *para*D_2–, and *ortho*D_2–CO_2 at a rotational temperature of $T=1.2\,K$ together with the available observed [145] spectra. It is shown that the calculated transition frequencies and line intensities are consistent with the available observed values. The transition 1_{01}–0_{00} is the strongest for *para*H_2–CO_2 and *ortho*D_2–CO_2, while 2_{02}–1_{01} is the strongest for *ortho*H_2–CO_2 and *para*D_2–CO_2. Significant isotopic effect was also revealed from our calculations. For H_2–CO_2, both *para*H_2–CO_2 and *ortho*H_2–CO_2 are mostly *a*-type transitions. For D_2–CO_2, however, only *a*-type transitions occur for *para*D_2–CO_2, whereas both *a*-type and *b*-type transitions are significant for *ortho*D_2–CO_2.

3.7. *H_2–OCS*

It has been identified that OCS is an ideal probe molecule for studies of helium clusters and nanodroplets [147–157, 159, 160]. In 2001, Grebenev *et al.* [150] formed the vdW clusters *para*H_2–, HD–, and *ortho*D_2–OCS inside mixed $^4He/^3He$ droplets and measured their high-resolution infrared spectra. The fully resolved rotational structure of the complexes was found to be that of an asymmetric top. The dependence of the rotational constants was used to determine the in-plane structure as well as the out-of-plane amplitude imposed by the superfluid liquid ^4He environment. Subsequently, they [151] analysed the high-resolution infrared spectra

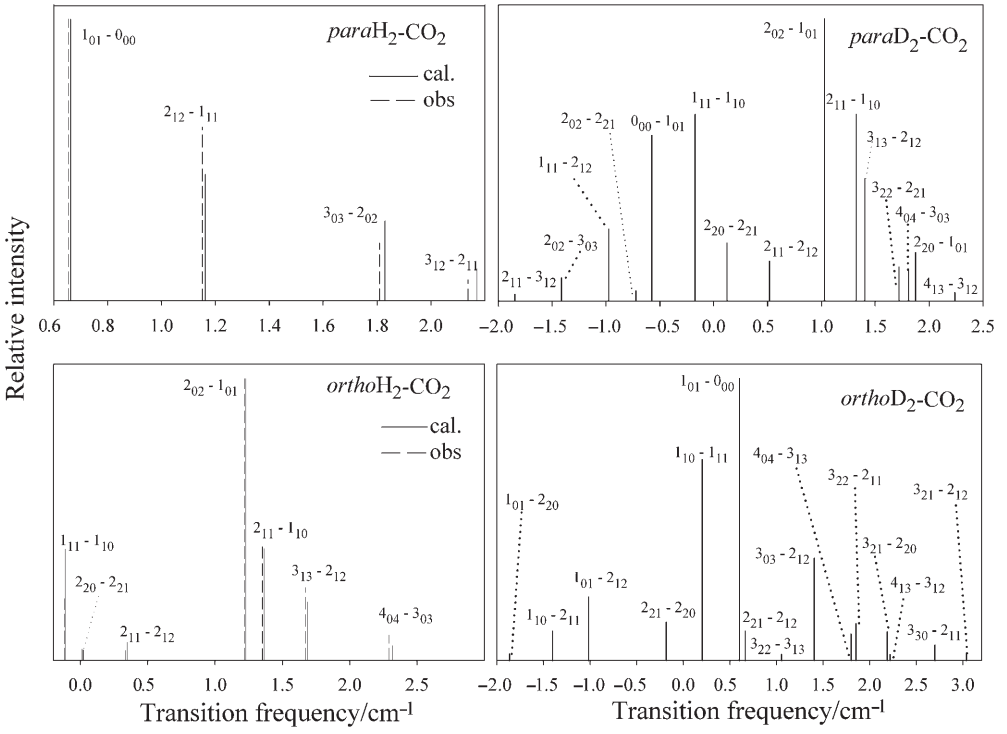

Figure 9. Calculated [145] and observed [145] line intensities for the H_2–CO_2 complexes. The transition frequencies are relative to the band origin.

of (*para*H_2)$_n$– and (*ortho*D_2)$_n$–OCS ($n = 2$–8) clusters inside an ultracold superfluid ^{4}He droplet coated with ^{3}He, and revealed the presence of highly symmetric five- and six-membered donut rings around the axis of the linear OCS from an analysis of the different Q-branch intensities based solely on their different nuclear spin symmetries of *para*H_2 and *ortho*D_2. Later, they [154] measured the high-resolution infrared spectra of the *para*H_2–, *ortho*H_2–, *ortho*D_2–, *para*D_2–, and HD–OCS vdW complexes in liquid helium droplets using diode laser droplet beam depletion spectroscopy. Tang and McKellar [143] observed the infrared spectra in the region of the OCS ν_3 vibration for five isolated species of H_2–OCS complexes in a pulsed supersonic jet expansion using a tunable diode laser probe, and found that the spectra contain only *a*-type transitions as those of prolate asymmetric rotors. The band origins are slightly red-shifted (-0.05 to $-0.20\,\mathrm{cm}^{-1}$) relative to that of the free OCS molecule. They [157] also studied the infrared spectra of (*para*H_2)$_n$–, (*ortho*H_2)$_n$–, and (HD)$_n$–OCS for $n = 2$–7 in the region of the C–O stretching vibration. Yu *et al.* [146] measured the rotational spectra of five isolated H_2–OCS complexes and revealed the intrinsic hyperfine interactions of hydrogen and the corresponding internal rotational dynamics.

Employing zero temperature quantum Monte Carlo methods, Paesani *et al.* [171] determined the structure and energetics of the (*p*araH_2)$_n$–OCS ($n = 1$–8) complexes. They carried out ground state calculations with importance-sampled rigid body diffusion Monte Carlo method and excited state calculations with the projection

Table 6. Calculated [13] first ten bound state energy levels (in cm^{-1}) with $J=0$ for complexes of OCS($v=0$) with different H_2 isotopomers.

n	*para*H_2	*ortho*H_2	*para*D_2	*ortho*D_2	HD
1	−72.560	−85.672	−103.692	−89.519	−82.674
2	−44.232	−69.551	−85.947	−61.384	−54.362
3	−41.671	−61.699	−77.326	−52.882	−48.399
4	−34.561	−52.528	−69.994	−49.435	−43.003
5	−29.794	−45.767	−61.071	−42.090	−36.990
6	−26.258	−40.982	−57.242	−39.562	−34.716
7	−19.371	−40.094	−55.167	−36.202	−29.856
8	−14.849	−38.351	−50.471	−34.364	−26.644
9	−8.831	−36.064	−50.036	−28.567	−20.590
10	−4.615	−33.987	−49.473	−25.720	−17.409

operator imaginary time spectral evolution approach. The ground states are found to be highly structured, with a gradual build up of two axial rings as n increases to 8. Excited state calculations were made for a range of total cluster angular momentum values, and the rotational energy levels were fitted to obtain effective rotational and distortion constants of the clusters using a symmetric top Hamiltonian. Detailed analysis of these spectroscopic constants indicates that the complexes have an unusually rich variation in dynamical behaviour, with sizes $n=1$–2 showing near rigid behaviour, sizes $n=3$–4 showing extremely floppy behaviour, and the larger sizes $n=5$–8 showing more rigid behaviour again. The large values of the distortion constant obtained for $n=3$–4 are rationalized in terms of the coupling between the OCS rotations and the 'breathing' mode of the first, partially filled ring of *para*H_2 molecules. They [172] later extended this study to larger (*p*araH_2)$_n$–OCS clusters with $n=9$–17. The dependence of the effective rotational constant on the cluster size shows near-rigid behaviour for clusters up to $n=13$, after which a significant departure from the rigid coupling between OCS rotations and *p*araH_2 motion appears.

In 2006, Paesani and Whaley [13] presented a five-dimensional PES for the H_2–OCS system that includes explicit dependence on the Q_3 normal vibration of the OCS molecule. The potential energies were calculated using the MP4 method with aVTZ basis set supplemented with a set of bond functions. The global minimum was found to locate at $R=3.23$ Å, $\theta_1=109.4°$, $\theta_2=93.0°$, and $\varphi=0.0°$ with the well depth of $-201.67\,cm^{-1}$. The global minimum region is very narrow along the θ_1 coordinate while it is considerably broader in the H_2 angle θ_2. In order to obtain the explicit dependence of the H_2–OCS interaction on a specific vibrational state of the OCS molecule, they integrated the five-dimensional PES over the Q_3 coordinate to generate two vibrationally adiabatic PESs, which were then used to calculate the bound state energies for the H_2–OCS complexes in both ground ($v=0$) and first excited ($v=1$) states of OCS by using the BOUND code [175] in which the close-coupling equations are numerically solved as described in [176]. Table 6 gives the energy levels for the first ten pure vibrational bound states for the five isotopomers with OCS at its $v=0$ state, and table 7 presents the dissociation energies and ZPEs for all H_2–OCS complexes with OCS at $v=0$ state. It is evident that the OCS complexes with H_2 isopomers for which only odd values of angular momentum j_2 are allowed (*ortho*H_2 and *para*D_2) have significantly greater binding energies than those complexes with H_2 isopomers

Table 7. Calculated [13] dissociation energy (D_0), zero-point energy (ZPE), and shift of the band origin ($\triangle\nu$) for five species of H_2–OCS. Experimental data from [143]. All energies in cm^{-1}.

Complex	D_0	ZPE	$\Delta\nu$	
			Theory	Experiment
paraH_2–OCS	72.5596	129.1147	−0.2099	−0.2049
orthoH_2–OCS	85.6718	116.0025	−0.1824	−0.0940
paraD_2–OCS	103.6919	97.9825	−0.1659	−0.0461
orthoD_2–OCS	89.5194	112.1550	−0.1989	−0.1588
HD–OCS	82.6739	119.0004	−0.2063	−0.1871

possessing only even j_2 values (*para*H_2 and *ortho*D_2). This was explained by checking the dependence of the PES on the H_2 relative molecular orientation. Table 7 shows that for these complexes the ZPE represents from 51% to 64% of the well depth of the PES.

The rovibrational transition energies for all H_2–OCS complexes were computed upon the two vibrationally averaged potential surfaces. Very good agreement with the observed data is found for all the transition energies, with the calculated values showing a slight shift of about $0.08\,cm^{-1}$ towards smaller frequencies. As given in table 6, the calculated [13] shift of the band origin is in excellent agreement with the observed [143] value for *para*H_2–, *ortho*D_2–, and HD–OCS, while the absolute value for *ortho*H_2– and *para*D_2–OCS is overestimated. The overall agreement indicates that the PESs accurately describe the interaction of a vibrating OCS molecule with different H_2 isotopmers.

4. Conclusions

It is now feasible to obtain the high-quality intermolecular pair potentials thanks to growing computer power and more sophisticated *ab initio* theories. Accurate PESs of vdW complexes become increasingly important because of their wide applications. Many reliable IPESs with the rigid monomer model have been constructed using either the supermolecular methods or the SAPT. The quality of the PESs is verified by comparing with their high-resolution spectra. Up to date, theoretical studies including explicitly the intramolecular degrees of freedom are still rather scarce, except for some simple atom–diatom complexes. Recently, quantum dynamical methods to treat large amplitude motions in the complex can arrive at up to six fully coupled degrees of freedom. It now thus becomes possible to include the explicit dependence of the intramolecular degrees of freedom in the studies of the rovibrational spectra of the complex.

In this review, we have summarized our very recent studies on the constructions of PESs and the calculations of the rovibrational bound states and transition intensities for the Rg– and H_2–(linear molecule) vdW complexes. In our studies, the PODVR grid points were used to represent the intramolecular vibrational coordinate Q. The potential at the coordinate Q is directly incorporated into the DVR Hamiltonian so that the fitting for the coordinate Q is completely avoided. With the explicit involvement of one intramolecular vibrational coordinate that is related to the transition in the infrared spectra, full prediction of the infrared spectra including the shift of band origin can be achieved. In the case of very small off-diagonal coupling, the vibrationally averaged

potentials for the ground and excited intramolecular vibrational states can be evaluated separately upon the *ab initio* points based on the PODVR grid points, so that the fittings of the potential and dipole moments for the coordinate Q are not required. The vibrationally averaged potentials are essential to simulate the spectroscopic properties of the related vdW clusters. Further developments will be directed to establish theoretical models for studying vdW complexes containing a non-linear molecule or an open-shell linear molecule.

Acknowledgements

This work was supported by the National Natural Science Foundation of China (Grant Nos. 20533060 and 10574068).

References

[1] A. van der Avoird, P. E. S. Wormer, and R. Moszynski, Chem. Rev. **94,** 1931 (1994).
[2] P. E. S. Wormer and A. van der Avoird, Chem. Rev. **100,** 4109 (2000).
[3] G. Chalasinski and M. M. Szczesniak, Chem. Rev. **100,** 4227 (2000).
[4] R. J. Le Roy and J. van Kranendonk, J. Chem. Phys. **61,** 4750 (1974).
[5] J. Tennyson and B. T. Sutcliffe, J. Chem. Phys. **77,** 4061 (1982).
[6] T. B. Pedersen, J. L. Cacheiro, B. Fernandez, and H. Koch, J. Chem. Phys. **117,** 6562 (2002).
[7] T. G. A. Heijmen, R. Moszynski, P. E. S. Wormer, and A. van der Avoird, J. Chem. Phys. **107,** 9921 (1997).
[8] R. Moszynski, B. Jeziorski, P. E. S. Wormer, and A. van der Avoird, Chem. Phys. Lett. **221,** 161 (1994).
[9] J. M. Hutson, J. Chem. Phys. **96,** 6752 (1992).
[10] R. J. Le Roy and J. M. Hutson, J. Chem. Phys. **86,** 837 (1987).
[11] M. Meuwly and J. M. Hutson, J. Chem. Phys. **119,** 8873 (2003).
[12] H. Jiang, M. Xu, J. M. Hutson, and Z. Bacic, J. Chem. Phys. **123,** 054305 (2005).
[13] F. Paesani and K. B. Whaley, Mol. Phys. **104,** 61 (2006).
[14] A. C. Peet and W. Yang, J. Chem. Phys. **91,** 6598 (1989).
[15] Z. Bacic and J. C. Light, J. Chem. Phys. **85,** 4594 (1986).
[16] S. E. Choi and J. C. Light, J. Chem. Phys. **90,** 2593 (1989).
[17] K. Raghavachari, G. W. Trucks, J. A. Pople, and M. Head-Gordon, Chem. Phys. Lett. **157,** 479 (1989).
[18] D. E. Woon and T. H. Dunning, J. Chem. Phys. **98,** 1358 (1993).
[19] D. E. Woon and T. H. Dunning, J. Chem. Phys. **100,** 2975 (1994).
[20] T. B. Pedersen, B. Fernandez, H. Koch, and J. Makarewicz, J. Chem. Phys. **115,** 8431 (2001).
[21] F. M. Tao, J. Chem. Phys. **98,** 3049 (1993).
[22] F. M. Tao and W. Klemperer, J. Chem. Phys. **101,** 1129 (1994).
[23] F. M. Tao, S. Drucker, R. C. Cohen, and W. Klemperer, J. Chem. Phys. **101,** 8680 (1994).
[24] F. M. Tao, Int. Rev. Phys. Chem. **20,** 617 (2001).
[25] S. F. Boys and F. Bernardi, Mol. Phys. **19,** 553 (1970).
[26] B. Jeziorski, R. Moszynski, and K. Szalewicz, Chem. Rev. **94,** 1887 (1994).
[27] F. B. van Duijneveldt, J. G. C. M. van Duijneveldt-van de Rijdt, and J. H. van Lenthe, Chem. Rev. **94,** 1873 (1994).
[28] K. Szalewicz and B. Jeziorski, in *Molecular Interactions – From van der Waals to Strongly Bound Complexes*, edited by S. Schiener (Wiley, New York, 1997).
[29] W. R. Rodwell, L. T. Sim Fai Lam, and R. O. Watts, Mol. Phys. **44,** 225 (1981).
[30] C. M. Lovejoy and D. J. Nesbitt, J. Chem. Phys. **93,** 5387 (1990).
[31] R. Moszynski, P. E. S. Wormer, B. Jeziorski, and A. van der Avoird, J. Chem. Phys. **101,** 2811 (1994).
[32] R. Moszynski, B. Jeziorski, A. van der Avoird, and P. E. S. Wormer, J. Chem. Phys. **101,** 2825 (1994).
[33] V. F. Lotrich, H. L. Williams, K. Szalewicz, B. Jeziorski, R. Moszynski, P. E. S. Wormer, and A. van der Avoird, J. Chem. Phys. **103,** 6076 (1995).
[34] G. Chalasinski, M. M. Szczesniak, and B. Kukawska-Tarnawska, J. Chem. Phys. **94,** 6677 (1991).
[35] J. M. Hutson, J. Chem. Phys. **88,** 4550 (1988).
[36] G. S. Yan, M. H. Yang, and D. Q. Xie, J. Chem. Phys **109,** 10284 (1998).

[37] F. Negri, F. Ancliotto, G. Mistura, and F. Toigo, J. Chem. Phys. **111,** 6439 (1999).
[38] F. Paesani and K. B. Whaley, J. Chem. Phys. **121,** 4180 (2004).
[39] H. Zhu, Y. Guo, Y. Xue, and D. Q. Xie, J. Comp. Chem. **27,** 1045 (2006).
[40] G. S. Yan, M. H. Yang, and D. Q. Xie, Chem. Phys. Lett. **275,** 494 (1997).
[41] G. S. Yan, M. H. Yang, and D. Q. Xie, Chem. Phys. Lett. **287,** 162 (1998).
[42] H. Zhu, Y. Z. Zhou, and D. Q. Xie, J. Chem. Phys. **122,** 234312 (2005).
[43] B. T. Chang, O. A-Ojo, R. Bukowski, and K. Szalewicz, J. Chem. Phys. **119,** 11654 (2003).
[44] Y. Z. Zhou and D. Q. Xie, J. Chem. Phys. **120,** 8575 (2004).
[45] X. G. Song, Y. J. Xu, P. N. Roy, and W. Jager, J. Chem. Phys. **121,** 12308 (2004).
[46] H. Zhu, D. Xie, and G. Yan, Chem. Phys. Lett. **351,** 149 (2002).
[47] H. Zhu, D. Q. Xie, and G. S. Yan, J. Comp. Chem. **24,** 1839 (2003).
[48] R. J. Doyle, D. M. Hirst, and J. M. Hutson, J. Chem. Phys. **125,** 184312 (2006).
[49] G. Murdachaew, A. J. Misquitta, R. Bukowski, and K. Szalewicz, J. Chem. Phys. **114,** 764 (2001).
[50] D. Cappelletti, M. Bartolomei, E. Carmona-Novillo, F. Pirani, G. Blanquet, and F. Thibault, J. Chem. Phys. **126,** 064311 (2007).
[51] O. Akin-Ojo, R. Bukowski, and K. Szalewicz, J. Chem. Phys. **119,** 8379 (2003).
[52] Y. Z. Zhou and D. Q. Xie, J. Chem. Phys. **122,** 174321 (2005).
[53] A. Huckauf, W. Jager, P. Botschwina, and R. Oswald, J. Chem. Phys. **119,** 7749 (2003).
[54] Y. Z. Zhou and D. Q. Xie, J. Chem. Phys. **121,** 2630 (2004).
[55] A. R. W. McKellar and H. L. Welsh, J. Chem. Phys. **55,** 595 (1971).
[56] J. Tennyson and B. T. Sutcliffe, J. Chem. Phys. **79,** 43 (1983).
[57] M. Jeziorska, P. Jankowski, K. Szalewicz, and B. Jeziorski, J. Chem. Phys. **113,** 2957 (2000).
[58] G. C. Groenenboom and I. M. Struniewicz, J. Chem. Phys. **113,** 9562 (2000).
[59] C. Bissonnette, C. E. Chuaqui, K. G. Crowell, R. J. Le Roy, R. J. Wheatley, and W. J. Meath, J. Chem. Phys. **105,** 2639 (1996).
[60] Y. Z. Zhou and D. Q. Xie, J. Chem. Phys. **123,** 134323 (2005).
[61] W. Klopper, M. Quack, and M. A. Suhm, J. Chem. Phys. **108,** 10096 (1998).
[62] M. J. Elrod and R. J. Saykally, J. Chem. Phys. **103,** 933 (1995).
[63] P. R. Bunker, V. C. Epa, P. Jensen, and A. Karpfen, J. Mol. Spectrosc. **146,** 200 (1991).
[64] R. J. Le Roy and J. S. Carley, Adv. Chem. Phys. **42,** 353 (1980).
[65] R. J. Le Roy, G. C. Corey, and J. M. Hutson, Faraday Discuss. Chem. Soc. **73,** 339 (1982).
[66] P. Jankowski, J. Chem. Phys. **121,** 1655 (2004).
[67] J. M. Hutson, J. Phys. Chem. **96,** 4237 (1992).
[68] J. Tennyson and B. T. Sutcliffe, Mol. Phys. **51,** 887 (1984).
[69] S. E. Choi and J. C. Light, J. Chem. Phys. **92,** 2129 (1990).
[70] Y. Z. Zhou, D. Q. Xie, and D. H. Zhang, J. Chem. Phys. **124,** 144317 (2006).
[71] H. Wei and T. Carrington, J. Chem. Phys. **97,** 3029 (1992).
[72] D. T. Colbert and W. H. Miller, J. Chem. Phys. **96,** 1982 (1992).
[73] J. Echave and D. C. Clary, Chem. Phys. Lett. **190,** 225 (1992).
[74] G. H. Golub and C. F. VanLoan, edn, Matrix Computations, 2nd ed. (The Johns Hopkins University Press, Baltimore, 1989).
[75] C. Lanczos, J. Res. Natl. Bur. Stand. **45,** 255 (1950).
[76] C. C. Paige, J. Inst. Math. Appl. **10,** 373 (1972).
[77] B. N. Parlett, *The Symmetric Eigenvalue Problem* (Prentice-Hall, Englewood Cliffs, 1980).
[78] J. K. Cullum and R. A. Willoughby, *Lanczos Algorithms for Large Symmetric Eigenvalue Computations* (Birkhauser, Boston, 1985).
[79] R. Chen and H. Guo, Chem. Phys. Lett. **277,** 191 (1997).
[80] R. Q. Chen and H. Guo, J. Chem. Phys. **119,** 5762 (2003).
[81] X. G. Wang and T. Carrington, J. Chem. Phys. **117,** 6923 (2002).
[82] J. C. Tremblay and T. Carrington, J. Chem. Phys. **125,** 094311 (2006).
[83] H. Li, D. Q. Xie, and H. Guo, J. Chem. Phys. **120,** 4273 (2004).
[84] C. X. Xu, D. Q. Xie, D. H. Zhang, S. Y. Lin, and H. Guo, J. Chem. Phys. **122,** 244305 (2005).
[85] H. Guo, R. Q. Chen, D. Q. Xie, and J. Theor., Comp. Chem. **1,** 173 (2002).
[86] G. Murdachaew, A. J. Misquitta, R. Bukowski, and K. Szalewicz, J. Chem. Phys. **114,** 764 (2001).
[87] R. Bukowski, J. Sadlej, B. Jeziorski, P. Jankowski, K. Szalewicz, S. A. Kucharski, H. L. Williams, and B. M. Rice, J. Chem. Phys. **110,** 3785 (1999).
[88] A. J. Misquitta, R. Bukowski, and K. Szalewicz, J. Chem. Phys. **112,** 5308 (2000).
[89] K. T. Tang and J. P. Toennies, J. Chem. Phys. **80,** 3726 (1984).
[90] C. R. Le Sueur, S. Miller, J. Tennyson, and B. T. Sutcliffe, Mol. Phys. **76,** 1147 (1992).
[91] P. Jensen and V. Spirko, J. Mol. Spectrosc. **118,** 208 (1986).
[92] A. Kudian, H. L. Welsh, and A. Watanabe, J. Chem. Phys. **43,** 3397 (1965).
[93] A. Kudian, H. L. Welsh, and A. Watanabe, J. Chem. Phys. **47,** 1553 (1967).

[94] A. R. W. McKellar, J. Chem. Phys. **61,** 4636 (1974).
[95] A. R. W. McKellar, J. Chem. Phys. **105,** 2628 (1996).
[96] A. R. W. McKellar, J. Chem. Phys. **122,** 084320 (2005).
[97] H. L. Williams, K. Szalewicz, B. Jeziorski, R. Moszynski, and S. Rybak, J. Chem. Phys. **98,** 1279 (1993).
[98] H. Wei, R. J. Le Roy, R. Wheatley, and W. J. Meath, J. Chem. Phys. **122,** 084321 (2005).
[99] P. J. Dunlop, H. L. Robjohns, and C. M. Bignell, J. Chem. Phys. **86,** 2922 (1987).
[100] S. J. Harris, S. E. Novick, and W. Klemperer, J. Chem. Phys. **60,** 3208 (1974).
[101] T. A. Dixon, C. H. Joyner, F. A. Baiocchi, and W. Klemperer, J. Chem. Phys. **74,** 6539 (1981).
[102] M. R. Keenan, L. W. Buxton, E. J. Campbell, A. C. Legon, and W. H. Flygare, J. Chem. Phys. **74,** 2133 (1981).
[103] P. A. Stockman and G. A. Blake, J. Chem. Phys. **98,** 4307 (1993).
[104] C. M. Lovejoy, M. D. Schuder, and D. J. Nesbitt, J. Chem. Phys. **85,** 4890 (1986).
[105] C. M. Lovejoy, M. D. Schuder, and D. J. Nesbitt, Chem. Phys. Lett. **127,** 374 (1986).
[106] C. M. Lovejoy and D. J. Nesbitt, J. Chem. Phys. **91,** 2790 (1989).
[107] C. M. Lovejoy, J. M. Hutson, and D. J. Nesbitt, J. Chem. Phys. **97,** 8009 (1992).
[108] G. T. Fraser and A. S. Pine, J. Chem. Phys. **85,** 2502 (1986).
[109] Z. S. Huang, K. W. Jucks, and R. E. Miller, J. Chem. Phys. **85,** 6905 (1986).
[110] J. T. Farrell Jr, O. Sneh, A. McIlroy, A. E. W. Knight, and D. J. Nesbitt, J. Chem. Phys. **97,** 7967 (1992).
[111] H. C. Chang and W. Klemperer, J. Chem. Phys. **98,** 2497 (1993).
[112] H. C. Chang, F. M. Tao, W. Klemperer, C. Healey, and J. M. Hutson, J. Chem. Phys. **99,** 9337 (1993).
[113] C. C. Chuang, S. N. Tsang, W. Klemperer, and H. C. Chang, J. Chem. Phys. **109,** 8836 (1998).
[114] C. C. Chuang, K. J. Higgins, H. C. Fu, and W. Klemperer, J. Chem. Phys. **112,** 7022 (2000).
[115] C. C. Chuang and W. Klemperer, J. Chem. Phys. **113,** 4116 (2000).
[116] M. A. Dvorak, S. W. Reeve, W. A. Burns, A. Grushow, and K. R. Leopold, Chem. Phys. Lett. **185,** 399 (1991).
[117] J. M. Hutson and B. J. Howard, Mol. Phys. **45,** 791 (1982).
[118] D. J. Nesbitt, M. S. Child, and D. C. Clary, J. Chem. Phys. **90,** 4855 (1989).
[119] L. J. Rawluk, M. Keil, M. H. Alexander, H. R. Mayne, and J. J. C. Barrett, Chem. Phys. Lett. **202,** 291 (1993).
[120] J. J. C. Barrett and H. R. Mayne, J. Chem. Phys. **100,** 304 (1994).
[121] A. McIlroy and D. J. Nesbitt, J. Chem. Phys. **97,** 6044 (1992).
[122] S. Y. Liu, Z. Bacic, J. W. Moskowitz, and K. E. Schmidt, J. Chem. Phys. **101,** 10181 (1994).
[123] S. Y. Liu, Z. Bacic, J. W. Moskowitz, and K. E. Schmidt, J. Chem. Phys. **103,** 1829 (1995).
[124] A. Ernesti and J. M. Hutson, J. Chem. Phys. **106,** 6288 (1997).
[125] M. R. Ghayal and E. Curotto, J. Chem. Phys. **111,** 5522 (1999).
[126] J. M. Hutson, S. Y. Liu, J. W. Moskowitz, and Z. Bacic, J. Chem. Phys. **111,** 8378 (1999).
[127] M. R. Ghayal and E. Curotto, J. Chem. Phys. **113,** 4298 (2000).
[128] E. Curotto, J. Chem. Phys. **114,** 4533 (2001).
[129] J. H. Skone and E. Curotto, J. Chem. Phys. **117,** 7137 (2002).
[130] I. N. Kozin, M. M. Law, J. M. Hutson, and J. Tennyson, J. Chem. Phys. **118,** 4896 (2003).
[131] M. F. Russo Jr, and E. Curotto, J. Chem. Phys. **120,** 2110 (2004).
[132] W. Kolos, G. Corongiu, and E. Clementi, Int. J. Quantum Chem. **17,** 775 (1980).
[133] P. J. Crutzen, Angew., Chem. Int. Ed. Engl. **35,** 1758 (1996).
[134] M. S. Ngari and W. Jager, J. Mol. Spectrosc. **192,** 320 (1998).
[135] K. Nauta and R. E. Miller, J. Chem. Phys. **115,** 10254 (2001).
[136] Y. J. Xu, W. Jager, J. Tang, and A. R. W. McKellar, Phys. Rev. Lett. **91,** 163401 (2003).
[137] J. Tang and A. R. W. McKellar, J. Chem. Phys. **117,** 2586 (2002).
[138] T. Korona, R. Moszynski, F. Thibault, J.-M. Launay, B. Bussery-Honvault, J. Boissoles, and P. E. S. Wormer, J. Chem. Phys. **115,** 3074 (2001).
[139] X. G. Wang, J. T. Carrington, J. Tang, and A. R. W. McKellar, J. Chem. Phys. **123,** 034301 (2005).
[140] F. Paesani and K. B. Whaley, J. Chem. Phys. **121,** 5293 (2004).
[141] D. E. Bernholdt, S. Y. Liu, and C. E. Dykstra, J. Chem. Phys. **85,** 5120 (1986).
[142] D. C. Clary and P. J. Knowles, J. Chem. Phys. **93,** 6334 (1990).
[143] J. Tang and A. R. W. McKellar, J. Chem. Phys. **116,** 646 (2002).
[144] J. Tang and A. R. W. McKellar, J. Chem. Phys. **117,** 8308 (2002).
[145] A. R. W. McKellar, J. Chem. Phys. **122,** 174313 (2005).
[146] Z. H. Yu, K. J. Higgins, W. Klemperer, M. C. McCarthy, and P. Thaddeus, J. Chem. Phys. **123,** 221106 (2005).
[147] S. Grebenev, J. P. Toennies, and A. F. Vilesov, Science **279,** 2083 (1998).
[148] S. Grebenev, M. Hartmann, M. Havenith, B. Sartakov, J. P. Toennies, and A. F. Vilesov, J. Chem. Phys. **112,** 4485 (2000).

[149] S. Grebenev, M. Havenith, F. Madeja, J. P. Toennies, and A. F. Vilesov, J. Chem. Phys. **113,** 9060 (2000).
[150] S. Grebenev, B. G. Sartakov, J. P. Toennies, and A. F. Vilesov, J. Chem. Phys. **114,** 617 (2001).
[151] S. Grebenev, B. Sartakov, J. P. Toennies, and A. F. Vilesov, Phys. Rev. Lett. **89,** 225301 (2002).
[152] M. Kunze, P. R. L. Markwick, N. Portner, J. Reuss, and M. Havenith, J. Chem. Phys. **116,** 7473 (2002).
[153] J. Tang, Y. Xu, A. R. W. Mckellar, and W. Jager, Science **297,** 2030 (2002).
[154] S. Grebenev, B. Sartakov, and J. P. Toennies, J. Chem. Phys. **118,** 8656 (2003).
[155] J. Tang and A. R. W. Mckellar, J. Chem. Phys. **119,** 5467 (2003).
[156] Y. Xu and W. Jager, J. Chem. Phys. **119,** 5457 (2003).
[157] J. Tang and A. R. W. McKellar, J. Chem. Phys. **121,** 3087 (2004).
[158] J. Tang and A. R. W. McKellar, J. Chem. Phys. **123,** 114314 (2005).
[159] C. Piccarreta and F. A. Gianturco, Eur. Phys. J. D **37,** 93 (2006).
[160] M. Y. Choi, G. E. Douberly, T. M. Falconer, W. K. Lewis, C. M. Lindsay, J. M. Merritt, P. L. Stiles, and R. E. Miller, Int. Rev. Phys. Chem. **25,** 15 (2006).
[161] Y. Z. Zhou, H. Ran, and D. Q. Xie, J. Chem. Phys. **125,** 174310 (2006).
[162] H. Ran, Y. Z. Zhou, and D. Q. Xie, J. Chem. Phys., **126**, 204304 (2007).
[163] K. Takayangi, Adv. At. Mol. Phys. **1,** 149 (1965).
[164] S. Y. Lin and H. Guo, J. Chem. Phys. **117,** 5183 (2002).
[165] G. C. Corey and D. Lemoine, J. Chem. Phys. **97,** 4115 (1992).
[166] D. Lemoine, J. Chem. Phys. **101,** 10526 (1994).
[167] D. T. Colbert and E. L. Sibert, J. Chem. Phys. **94,** 6519 (1991).
[168] M. J. Bramley and T. Carrington, J. Chem. Phys. **99,** 8519 (1993).
[169] J. Antikainen, R. Friesner, and C. Leforestier, J. Chem. Phys. **102,** 1270 (1995).
[170] R. Q. Chen, G. B. Ma, and H. Guo, Chem. Phys. Lett. **320,** 567 (2000).
[171] F. Paesani, R. E. Zillich, and K. B. Whaley, J. Chem. Phys. **119,** 11682 (2003).
[172] F. Paesani, R. E. Zillich, Y. Kwon, and K. B. Whaley, J. Chem. Phys. **122,** 181106 (2005).
[173] P. Jankowski, S. N. Tsang, W. Klemperer, and K. Szalewicz, J. Chem. Phys. **114,** 8948 (2001).
[174] L. Wang, M. H. Yang, A. R. W. McKellar, and D. H. Zhang, Phys. Chem. Chem. Phys. **9,** 131 (2007).
[175] J. M. Hutson. BOUND computer program, version 5, distributed by Collaborative Computational Project No. 6, UK Science and Engineering Research Council (1993).
[176] J. M. Hutson, Comp. Phys. Comm. **84,** 1 (1994).